Chapter 5
Application of Novel Carbonaceous Materials as Support for Fuel Cell Electrocatalysts

Abha Bharti and Gouri Cheruvally

Abstract Low-temperature fuel cells are potential candidates in alternative energy industry due to their high energy efficiencies and near zero emissions. Typically, carbon supported Pt-based materials are used as electrocatalysts for anode and cathode reactions in low-temperature fuel cells. Carbon black (CB) is the most commonly employed support material for Pt-based electrocatalysts. However, CB materials suffer from significant drawbacks such as poor corrosion resistance and limited mass transport of fuels to active catalyst sites. As an alternative to conventional CB support materials, carbon structures such as graphene, ordered mesoporous carbon, and the so-called green carbon have been successfully used in recent years as supports for the dispersion of fuel cell catalyst nanoparticles. This chapter briefly describes the newly developed carbonaceous nanostructures and their applications in low-temperature fuel cells.

Keywords Low-temperature fuel cells · PEMFC · DMFC · Carbonaceous support materials · Pt electrocatalysts · Oxygen reduction reaction · Methanol oxidation reaction · Carbon black · Graphene · Ordered mesoporous carbon · Green carbon · Synthesis techniques · Nanoparticles dispersion · Hard template · Soft template · CVD · Biomass · Chemical reduction · Surface functionalization · Hybrid nanocomposites

5.1 Introduction

The twenty-first century has witnessed tremendous increase in global energy demand, consequent to depletion of fossil fuel reserves and serious climate concerns due to emission of greenhouse gases, which has directed mankind to switch to alternate "greener" and sustainable energy sources. Towards this, fuel cells with

A. Bharti · G. Cheruvally (✉)
Propellants, Polymers, Chemicals and Materials Entity, Vikram Sarabhai Space Centre, Thiruvananthapuram, Kerala, India

F. J. Rodríguez-Varela, T. W. Napporn (eds.), *Advanced Electrocatalysts for Low-Temperature Fuel Cells*, https://doi.org/10.1007/978-3-319-99019-4_5

high energy conversion efficiencies and near zero emissions have emerged as prospective alternate energy conversion devices for portable, mobile, and stationary power applications [1–3]. Fuel cells are electrochemical devices which are capable of converting chemical energy of "fuels" directly into electrical energy surpassing the intermediate stages of heat generation and mechanical work (Carnot's cycle), typical of conventional power generation methods. Thus, fuel cells are devoid of thermodynamic limitations of heat engines, and hence, are more efficient [4]. Low-temperature fuel cells, particularly proton exchange membrane fuel cells (PEMFCs) and direct methanol fuel cells (DMFCs) are considered the most effective and environmentally sustainable power sources because of their simple operation, high energy density, rapid start-up and shut-down cycle under ambient conditions, and high efficiency [5]. However, the effective commercialization of these classes of fuel cells is limited by the high usage of expensive Pt-based catalysts for electrochemical reactions at anode as well as cathode amounting to almost 27–43% of the cost of a fuel cell stack [6]. In addition, the sluggish kinetics of oxygen reduction reaction (ORR) at the cathode of both PEMFC and DMFC along with complex methanol oxidation reaction (MOR) and self-poisoning of Pt by intermediate products such as CO at anode in DMFC needs significant improvement for their wide scale applications. Furthermore, the methanol crossover from anode to cathode in DMFC hampers the ORR performance due to simultaneous methanol oxidation and oxygen reduction resulting in mixed potential losses at cathode. Hence, it is imperative to develop electrocatalysts with improved catalytic activities and lower Pt content to realize the real commercialization of fuel cells.

It is well known that significant enhancement in electrocatalytic activity can be achieved by dispersion of Pt-based catalysts on nanostructured support materials with additional advantage of reduced noble metal consumption [7, 8]. In this regard, a good catalyst support should have large surface area for dispersion of catalyst particles, good electrical conductivity, and high electrochemical stability [7]. Moreover, the nature of supporting materials and synergistic interactions between metal nanoparticles (NPs) and support greatly influence the catalyst performance [9, 10]. Hence, the selection of suitable supporting materials is vital for the development of fuel cell technology. The most commonly employed support materials for Pt-based catalysts in low-temperature fuel cells are carbonaceous materials, specifically carbon black (CB, Vulcan XC-72) because of its large surface area, high electronic conductivity, and easy availability [11]. However, CB suffers from severe disadvantages such as poor electrochemical stability/corrosion resistance and mass transport limitation due to the presence of micropores less than 1 nm which hinders fuel supply to the reactive sites limiting the catalytic activity. The large number of micropores also results in low accessible surface area for the deposition of metal NPs leading to a lower electrochemical surface area (ESA) and poor catalytic activity. Therefore, various alternatives to CB support materials are being searched extensively.

Recently, nanostructured carbon materials such as graphene [6], networked mesostructured porous carbon materials, specifically ordered mesoporous carbons (OMCs) [12], and green carbons, *i.e.*, the carbon derived from renewable resources

(biomass), have emerged as promising support materials for low-temperature fuel cells [13]. The higher catalytic activity of the Pt-based catalysts supported on these nanostructured carbon supports than that of the same catalysts supported on CBs has been ascribed to a combination of their unique structures and properties such as high surface area, good electronic conductivity, chemical stability, and synergistic metal–support interactions. This chapter presents an overview of synthesis techniques of graphene, OMCs, and green carbons together with the application of these newly developed carbonaceous structures as support materials for low-temperature fuel cells.

5.2 Graphene

Graphene is a single atom thin sheet of sp^2 hybridized, hexagonally arranged carbon atoms in a honeycomb lattice and derives its name from the combination of graphite and alkene [14]. This remarkable two-dimensional (2D) material has aroused tremendous interest for further pursuance because of its many unique properties such as high specific surface area (SSA, theoretical value of 2630 $m^2\ g^{-1}$), superior electronic conductivity (10^3–10^4 S m^{-1}), robust mechanical properties, excellent stability, fast electron transfer capabilities, and low manufacturing cost [15]. Considering these exceptional attributes, graphene is being explored as a promising support material for Pt-based catalysts in low-temperature fuel cells. The 2D planar structure of graphene provides high surface area for deposition of the catalyst NPs which can interact through both the edge planes and basal planes of the carbon sheets. The presence of strong metal–support interaction in this planar structure also improves the stability of the nanocatalysts which is highly desirable for long duration operation of fuel cells. Since its discovery in 2004, graphene has been studied as a support material for fuel cell catalyst and evidenced tremendous advancement in this area of research during the past decade. In this section, the synthesis methodologies developed for this wonder material and graphene supported nanocatalysts are summarized. In addition, the catalytic activity and durability of catalysts supported on graphene are compared with those of catalysts supported on the commonly used CBs.

5.2.1 Synthesis Techniques

The first graphene sheets were obtained by extracting monolayer sheets from the three-dimensional graphite using Scotch tape method in 2004 [16]. Since then, different approaches have been explored for the production of monolayer graphene sheets from graphite [17–21]. Out of these, three primary methods have been reported to be quite successful. These include: (1) mechanical exfoliation, (2) chemical vapor deposition (CVD) onto metal or Si substrates, and (3) chemical,

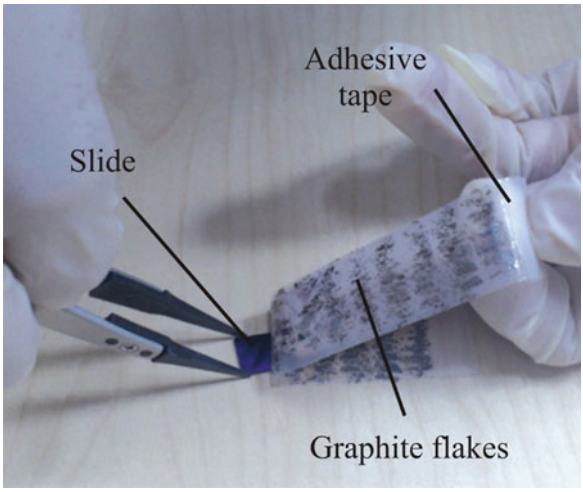

Fig. 5.1 Scotch tape procedure to get few-layer graphene. Reproduced with permission from Ref. [25], Copyright Nature, 2012

electrochemical, or thermal reduction of graphene oxide. Mechanical exfoliation is a top-down approach for preparing graphene with high carrier mobility (~10,000 cm^2 V^{-1} s^{-1}) and involves breaking apart of stacked layers of graphite to obtain single layer or few-layer sheets of graphene [22–24]. This micro-mechanical cleavage or more commonly, the scotch tape method, is quite straight-forward and requires no specialized equipment. The process typically involves placing of an adhesive tape onto the surface of graphite deposited on a silica slide and subsequently peeling it off to obtain thinner flakes (Fig. 5.1) [25, 26]. The whole process is repeated a number of times to obtain the desired graphene (single or few-layer) and is time consuming. Considering the inherent laborious process of this conventional micro-mechanical cleavage, Jayasena et al. introduced a novel lathe-like experimental setup utilizing ultra-sharp single crystal diamond wedge to cleave highly ordered pyrolytic graphite (HOPG) samples to produce few-layer graphene. Ultrasonic oscillations along the wedge assisted in cleaving HOPG for generating graphene flakes [27]. A modified scotch tape method-based exfoliation of natural graphite using three-roll mill machine with a polymer adhesive was reported by Chen et al. [28]. The employed polymer adhesive (polyvinyl chloride dissolved in dioctyl phthalate) has the same role as of tape adhesive in the original scotch tape method. The dispersion and exfoliation of graphite happen in the adhesive.

Graphene has been grown through CVD by high temperature pyrolysis of hydrocarbons using catalytic metals. CVD produces high quality graphene which can have high carrier mobility values, ~2000 to 4000 cm^2 V^{-1} s^{-1} [17]. The graphene growth via CVD can be categorized as proceeding either through surface catalyzed or segregation methods depending on the catalytic metal [21]. The solubility of the carbon containing species in the catalytic metal determines the dominant growth process. In surface catalyzed reactions, the decomposition of hydrocarbons occurs at metal surface and graphene growth is “self-limited” to monolayer. In the segregation method, the carbon dissolved in the bulk metal diffuses to the metal

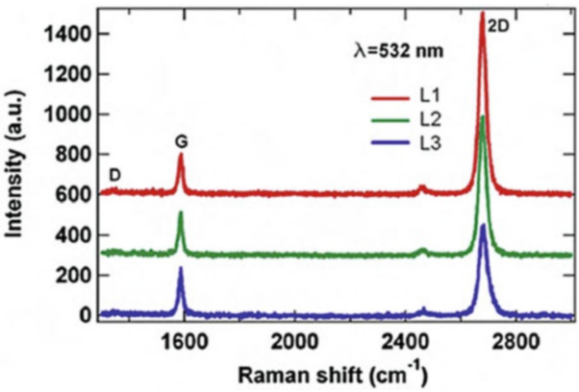

Fig. 5.2 Raman spectra of CVD graphene transferred to a Si/SiO_2 substrate. Reproduced with permission from Ref. [30], Copyright Elsevier, 2010

surface to produce graphene. CVD graphene growth is commonly performed using Cu and Ni catalysts [29]. Wu et al. reported wafer-scale synthesis of graphene on Cu foils by thermal CVD at a temperature of 1000 °C and under ambient pressure with methane as the precursor gas [30]. The Raman spectrum of graphene thus obtained (Fig. 5.2) showed I_{2D}/I_G ratio larger than 2, indicating formation of a monolayer. Van Nang et al. prepared few-layer graphene using Cu foil through inductively coupled plasma CVD within a duration of few seconds [31]. The authors demonstrated that the thickness of the graphene formed can be tuned by controlling the growth time and power of the plasma. Chae et al. reported synthesis of highly crystalline, large area graphene by CVD using poly-Ni substrate with C_2H_2/H_2 gas under optimized CVD conditions [32]. It was concluded that high temperature, short growth time, and an optimal gas mixing ratio were required to synthesize highly crystalline few-layer graphene.

Graphene can also be obtained via oxidation of graphite to graphene oxide which is based on many variations of the "Hummers method" invented by William Hummers in 1958 [33] and further reduction of graphene oxide to graphene. The Hummers method utilizes oxidation of graphite using powerful oxidizing agents and strong acids. The oxidation of the graphite results in an increase of interlayer spacing which facilitates the dispersion of graphene in appropriate solvents [23]. Also, the interlayer spacing is strongly dependent on the extent of oxidation of graphite and, hence, can be desirably tailored. The chemical oxidation of graphite produces graphene oxide which is further reduced through thermal, chemical, or electrochemical approach to get graphene. Iqbal and Abdala produced thermally reduced graphene (TRG) through thermal exfoliation of graphite oxide (GO) [34]. The oxidation of graphite was carried out through Staudenmaier method [35] using H_2SO_4, HNO_3, and potassium chlorate followed by rapid heating at 1000 °C in a tube furnace. TRG exhibited SSA of 210 $m^2\ g^{-1}$ and cumulative pore volume of 0.57 $cm^3\ g^{-1}$. The surface elemental composition analysis of TRG through X-ray photoelectron spectroscopy (XPS) revealed the presence of oxygen functional groups such as epoxy, hydroxyl, and carboxylic acid, which provides polar/hydrophilic nature to the graphene and assists in its dispersion in suitable solvents. In the

work of Choi et al., GO was first prepared by chemical oxidation of natural graphite with H_2SO_4, $K_2S_2O_8$, P_2O_5, and $KMnO_4$ [36]. The subsequent thermal exfoliation of GO at 830 °C under Ar atmosphere resulted in the formation of graphene nanosheets with surface oxygen functional groups (C–OH, C–O–C, and HO–C=O). A low-temperature hydrogen induced thermal exfoliation route was proposed by Kaniyoor et al. [37]. In contrast to conventional thermal exfoliation route, GO was exfoliated in the presence of hydrogen at a low temperature of 200 °C. Yan et al. also reported a low-temperature exfoliation method using $Mg(OH)_2$ nanosheets as template [38]. High surface area functionalized graphene nanosheets were obtained by heating the mixture of GO and $Mg(OH)_2$ at 300 °C for 2 h under N_2 atmosphere with a slow heating rate of 3 °C min^{-1}. Doping graphene with heteroatoms such as N, S, B, and P can effectively tune its electronic structure and other intrinsic properties which enhances its support characteristics [6, 39]. Sheng et al. reported synthesis of N-doped graphene through a facile, catalyst-free route by thermal annealing of GO and melamine (as nitrogen source) at 800 °C in a tubular furnace under Ar atmosphere [40]. Based on XPS analysis, a total of 10.1 wt.% of nitrogen was estimated in the graphene layers and the N 1s XPS spectrum showed that all nitrogen atoms were mostly in pyridine-like bonding configuration, which is known to improve electrocatalytic activity.

Utilizing chemical exfoliation of GO with hydrazine hydrate as reducing agent, Stankovich et al. prepared high surface area (466 $m^2 g^{-1}$) graphene nanosheets with good electrical conductivity (2×10^2 S m^{-1}) [41]. It was found that this reduction route resulted in the formation of unsaturated and conjugated carbon atoms which are responsible for imparting high electrical conductivity. Ramachandran et al. investigated the effect of concentration of reducing agent, $NaBH_4$ on synthesis, and properties of graphene from GO [42]. GO and $NaBH_4$ weight ratio was varied as 1:4, 1:8, 1:10, and 1:12 to prepare graphene by chemical exfoliation. Results demonstrated better reduction of GO and superior reduction of oxygen functional groups with the ratio of 1:10. Sridhar et al. employed a novel, microwave assisted chemical reduction approach to prepare graphene nanosheets [43]. In contrast to conventional chemical methods which utilize harsh oxidizers such as H_2SO_4/$KMnO_4$, here the reduction was carried out using eco-friendly chemicals (ammonium peroxy disulfate and hydrogen peroxide) and subsequent microwave irradiation resulted in rapid exfoliation of graphite. Wang et al. reported a low cost, scalable, and non-toxic green method for reduction of graphene oxide using green tea solution [44]. Chemical exfoliation of graphene oxide was achieved by utilizing the reducing capability and the aromatic rings of tea polyphenol (TP) in green tea. The strong interactions between the reduced graphene and the aromatic TPs imparted good dispersibility of the resultant graphene in both aqueous and a variety of organic solvents. The results also demonstrated efficient removal of the oxygen-containing groups in graphene oxide with TPs.

Electrochemical methods are also employed for the reduction of graphene oxide to remove the oxygen functionalities and improve the electronic properties of graphene formed. The electrochemical reduction of graphene oxide is typically carried out in a standard electrochemical cell with a non-hazardous aqueous

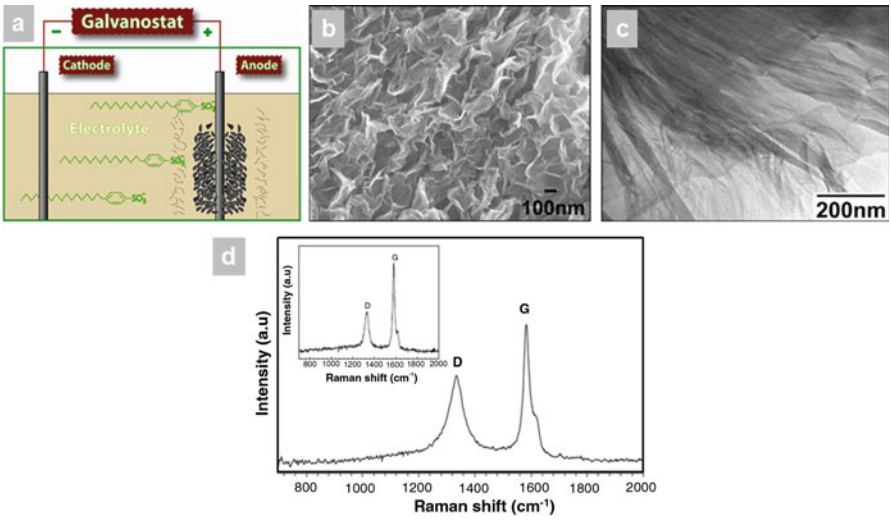

Fig. 5.3 (**a**) Experimental setup for synthesis of graphene via electrolytic exfoliation, (**b**) FESEM image of the bulk graphene powders, (**c**) TEM image of graphene sheets, and (**d**) Raman spectrum of the bulk graphene nanosheet powders. The inset is the Raman spectrum of the pristine graphite rod. Reproduced with permission from Ref. [47], Copyright Elsevier, 2009

electrolyte at room temperature with an applied potential [45]. The properties of the electrochemically reduced graphene oxide can be tuned by controlling the electrolysis parameters and electrolyte [46]. Wang et al. prepared graphene through electrolytic exfoliation of graphite using poly(sodium-4-styrenesulfonate) as an effective electrolyte [47]. A constant dc potential of 5 V was applied to two graphite rods placed in an electrolysis cell filled with the electrolyte and the electrolytic exfoliation continued for 4 h. The experimental setup is shown in Fig. 5.3a. The formation of monolayer graphene sheets and stacks containing a few-layer graphene sheets was confirmed through FESEM and TEM images (Fig. 5.3b, c, respectively). Furthermore, more intense G band as compared to D band was observed in the Raman spectrum shown in Fig. 5.3d indicating formation of graphene with a low defect content. Cooper et al. prepared few-layer graphene flakes of 2 nm thickness via the electrochemical intercalation of tetraalkylammonium cations into pristine graphite [48]. The electrochemical intercalation was carried out in a three electrode configuration with two types of working electrodes: HOPG and graphite rod. Tetramethylammonium perchlorate (TMA ClO_4), tetraethylammonium tetrafluoroborate (TEA BF_4), or tetrabutylammonium tetrafluoroborate (TBA BF_4) dissolved in 1-methyl-2-pyrrolidone were used as electrolytes. Significant electrode expansion had resulted with HOPD electrode than with graphite rod which was attributed to the high anisotropy of HOPG. It was also found that TBA was the most effective cation for HOPB electrode expansion, followed by TEA.

5.2.2 Application as Support and Dispersion of Metal Nanoparticles

Graphene is one of the most widely explored carbonaceous support materials for noble metal NPs. The hybrid nanocomposites of graphene with metal NPs are promising electrocatalysts for low-temperature fuel cells. The unique physicochemical properties of graphene such as 2D structure, high surface area with surface defects which acts as metal anchoring sites, and high electrical conductivity facilitate uniform dispersion of metal NPs onto its surface with strong metal–support interaction. This results in enhanced catalytic activity and durability of these hybrid electrocatalysts. The catalytic performance is significantly influenced by the size, composition, shape, and dispersion states of noble metal nanocrystals as well as their interactions with graphene support [6].

Metal NPs/graphene-based hybrid electrocatalysts are typically prepared by depositing metal precursors onto graphene-based support materials followed by their subsequent reduction adopting various methods [39]. Li et al. reported one pot synthesis of Pt nanoclusters with diameter of about 5–6 nm decorated graphene sheets via reduction of GO and Pt precursor with $NaBH_4$ [49]. The strong reducing agent facilitated in-situ reduction of reactants to form graphene and Pt-NPs and, thus, obtained Pt/Graphene nanocomposite. Compared to the conventional Pt/Vulcan catalyst, the Pt/Graphene nanocomposite demonstrated higher electrochemical surface area (ESA), better catalytic activity and stability for methanol oxidation. Jafri et al. used N-doped graphene (N-G) nano-platelets as support for Pt-NPs and studied their electrocatalytic properties. Graphene nano-platelets were synthesized by thermal exfoliation of GO and further treated in nitrogen plasma to produce nitrogen (3 at.%)-doped material [50]. Pt-NPs were dispersed on the support using the $NaBH_4$ reduction process to get the catalyst Pt/N–G. Membrane electrode assemblies (MEAs) fabricated using Pt/N–G and Pt/G as the ORR catalysts showed a maximum power density of 440 mW cm^{-2} and 390 mW cm^{-2}, respectively. The improved performance of Pt/N–G was attributed to the formation of pentagons and heptagons due to the incorporation of N in the C-backbone leading to increase in the conductivity of neighboring C atoms. In the work of Hsieh et al., Pt-NPs on graphene were formed from GO by two routes (one-step and two-step routes) [51]. For one-step route, a fixed weight of GO and a variable weight of $H_2PtCl_6{\cdot}6H_2O$ was used with ethylene glycol (EG) as the reducing agent. In the two-step route, the reduction of GO films was done initially to obtain graphene followed by deposition of Pt particles through EG reduction. The results showed that the Pt particles have smaller size and better distribution on the surface of graphene via two-step reduction route. The Pt/Graphene nanocomposites showed higher ESA (159.48 m^2 $g_{Pt}{}^{-1}$) and improved electrocatalytic activity towards the reduction of oxygen. The better results obtained were attributed to the very high Pt loading achieved and the small size of Pt-NPs dispersed uniformly on graphene nanosheets.

In recent years, microwave (MW) assisted processes have gained popularity to prepare metal NPs/graphene hybrids. MW irradiation offers homogeneous and rapid

heating which facilitates the formation of smaller and well-dispersed metal NPs [52, 53]. Zhao et al. fabricated a novel sandwich-structured graphene-Pt-graphene (G–P–G) catalyst through MW assisted polyol route using EG [54].The graphene support was first prepared by oxidation of graphite to GO by modified Hummers method. Subsequently, GO and Pt precursor were dispersed in EG/isopropyl alcohol solution (pH = 12) and subjected to continuous MW heating for 64 s which resulted in the formation of Pt-Graphene nanostructures. The sandwich G–P–G structures were formed by further addition of GO to Pt-Graphene dispersion followed by ultrasonic treatment and heating under Ar atmosphere at 140 °C for 1.5 h. Electrochemical results revealed superior MOR activity and stability with G–P–G catalyst which was attributed to facile metal support interaction due to anchoring of Pt-NPs between the two adjacent graphene sheets. Pt decorated, boron-doped graphene catalysts for ORR were prepared by Pullamsetty et al., following different chemical reduction methods by employing $NaBH_4$, EG, and mixture of $NaBH_4$ + EG (modified method) as reducing agent through conventional heating (CH) [55] as well as MW irradiation methods [56]. The study showed superior catalytic activity of boron-doped graphene-based catalysts prepared using the modified method following both CH and MW irradiation routes.

Oztuna et al. reported mesoporous graphene aerogel (GA) supported Pt-NPs prepared via supercritical deposition (SCD) using supercritical CO_2 ($scCO_2$), as ORR catalyst for PEMFC [57]. The Pt precursor was dissolved in $scCO_2$ and adsorbed onto GA at 35 °C and 10.7 MPa and was converted to its metal form under atmospheric pressure at different temperatures of 400 °C, 600 °C, and 800 °C. The effects of precursor conversion temperature on the structural properties of the composites and ORR activity were investigated. The results revealed that SCD helped to preserve the textural properties of the GA after the deposition of Pt-NPs, and Pt/GA converted at 600 °C exhibited an enhanced mass activity of 30.6 mA mg_{Pt}^{-1}, out-performing the mass activities reported in the literature for Pt/GA electrocatalysts prepared using conventional routes. Daş et al. investigated the effectiveness of two synthetic approaches: $scCO_2$ deposition and MW irradiation, to synthesize Pt-NPs uniformly dispersed on graphene nano-platelets (G) as catalyst support [58]. The study revealed formation of smaller Pt-NPs on G through $scCO_2$ deposition route (Pt/G2 1.5–1.6 nm) as compared to MW irradiation route (Pt/G1 3.1–3.4 nm). Pt/G2 catalyst exhibited higher ESA and fuel cell performance as compared to Pt/G1. The improved performance of the catalyst prepared via $scCO_2$ deposition route was attributed to the decrease in degree of agglomeration of Pt-NPs during the reduction process because of the higher interaction between adsorbed precursor ions and the graphene surface compared to the MW irradiation method. Pt/G2 also demonstrated higher corrosion resistance.

Electrochemical techniques have also been utilized for uniform dispersion of Pt-NPs on graphene-based support materials. Liu et al. utilized a "green" electrochemical approach to prepare nanocomposite films of Pt-NPs and graphene sheets [59]. First, expandable graphene oxide (EGO) support materials were prepared through modified Hummers and Offeman method using H_2SO_4, $KMnO_4$, and H_2O_2

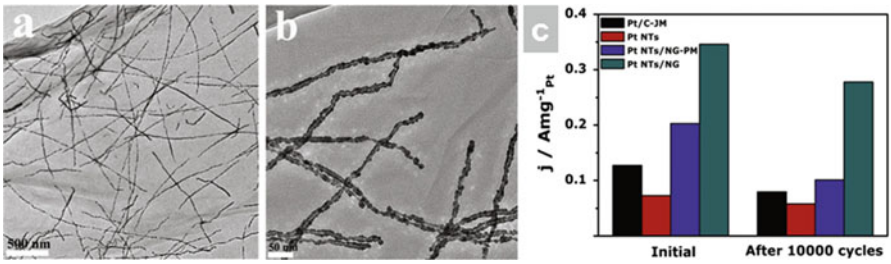

Fig.5.4 (**a**, **b**) TEM images of Pt NTs/NG catalyst and (**c**) mass activity of Pt-based catalysts before and after durability test. Reproduced with permission from Ref. [60], Copyright Elsevier, 2015

as oxidizing agents. Subsequently, electrophoretic deposition of EGO film on a conductive indium tin oxide surface was carried out at 150 V in constant potential mode. The deposited EGO film was in-situ electrochemically reduced using 0.1 M KCl to expandable graphene sheet (EGS). Finally, Pt-NPs were electrodeposited on the EGS film at a constant potential of −0.25 V for 1800 s in a mixed solution of 3 mM H_2PtCl_6 and 0.5 M H_2SO_4. Well-dispersed, uniform Pt-NPs with diameter of about 15 nm were distributed on EGS surface. Pt/EGS demonstrated better MOR activity than Pt-NPs deposited on glassy carbon. The improved electrocatalytic activity was attributed to the unique microstructure and surface topography of EGS and its synergistic interactions with the deposited Pt particles. Zhu et al. designed a strongly coupled Pt nanotubes/nitrogen-doped graphene (Pt NTs/NG) hybrid material utilizing galvanic replacement reaction between Te nanowires (NWs) and Pt precursors [60]. The Te NWs template resulted in the formation of one-dimensional (1D) tubular nanostructured Pt with an average diameter of 10.2 nm (Fig. 5.4a, b). The Pt NTs/NG demonstrated superior activity and durability towards ORR with a 2.7-fold improvement in mass activity (0.35 A mg^{-1} *vs.* 0.13 A mg^{-1}) as compared to commercial Pt/C catalyst. Pt NTs/NG catalyst also showed excellent durability characteristics and retained 88.9% of its initial activity after 10,000 cycles of accelerated durability tests (Fig. 5.4c).

Guo et al. fabricated 3D Pt on Pd bimetallic nanodendrites on graphene nanosheets (TP-BNGN) through a three step wet-chemical approach [61]. Poly(*N*-vinyl-2-pyrrolidone) (PVP) functionalized graphene was prepared first by ultrasonic exfoliation of GO with PVP solution followed by reduction with hydrazine and ammonia solution. In the next step, Pd NPs were deposited on PVP-functionalized graphene by HCOOH assisted chemical reduction. Finally, TP-BNGN catalyst was fabricated by mixing Pd NP/PVP-graphene with Pt precursor and subsequent metal reduction with ascorbic acid. The study demonstrated higher catalytic activity of TP-BNGNs than that of Pt/C (E-TEK) towards methanol electro-oxidation. The improved electrocatalytic activity was attributed to the three-dimensional (3D) bimetallic nanodendrites structure of Pt–Pd particles and their better dispersion on the graphene nanosheets with high surface area. Jafri et al. reported N-doped graphene as support for Pt-NPs that were synthesized using hydrothermal method and thermal solid state

method using two sources of nitrogen, ammonia and melamine, respectively [62]. The synthesized graphene-based catalysts were evaluated as ORR catalyst in both half-cell and full cell mode. In this work, MWCNT was used as a spacer and fuel cell results demonstrated enhanced performance with N-doped, graphene-based Pt catalyst prepared by hydrothermal method. This catalyst exhibited 1.5 times higher power density than commercial Pt/C catalyst (704 mW cm^{-2} *vs.* 460 mW cm^{-2}), establishing it as a promising cathode catalyst for PEMFC.

5.3 Ordered Mesoporous Carbons

Ordered mesoporous carbons (OMCs) belong to the family of carbon materials with pore size of 2–50 nm. OMCs are made up of periodically aligned arrays of mesopores with narrow pore size distribution forming a highly interconnected network. This novel carbonaceous material was discovered in the year 1999 by Ryoo et al. [63] and since then has witnessed a sudden upsurge of interest among the scientific community for its various applications, particularly in the field of energy storage and conversion [64]. Specifically, OMCs have garnered enormous attention as support materials for low-temperature fuel cells due to their unique properties such as high SSA, good electrical conductivity, large numbers of three dimensionally connected, mono-dispersed mesopores which facilitate diffusion of reactants, and by-products from the active sites contributing to catalysis [7, 65]. Additionally, they are also known to possess surface oxygen groups which are considered to improve the interaction between the metal catalyst and the carbon support allowing better dispersion; this also imparts better activity and durability. This section is focused on the synthesis methodology of OMCs, their suitability and application as support materials for low-temperature fuel cells.

5.3.1 Synthesis of OMCs

The story of OMCs started with the pioneering work of Ryoo et al. [63] where ordered mesoporous silica molecular sieve, Mobil Crystalline Matter/Mobil Composite Matter-48; MCM-48, was used as template along with sucrose as carbon source and sulfuric acid as the catalyst. The template was impregnated with the aqueous solution of sucrose and heated in the temperature range of 1073–1373 K under vacuum or inert atmosphere followed by conversion to carbon using sulfuric acid catalyst. Finally, the template was removed using aqueous solutions of NaOH and ethanol, which resulted in the formation of ordered porous carbon materials referred to as CKM-1. The authors demonstrated the applicability of this silica template-based synthetic route for large industrial applications. After 19 years of concerted efforts, significant development in the field of synthesis of these "unique" OMC materials has been realized [66–72] and OMCs with various mesostructures,

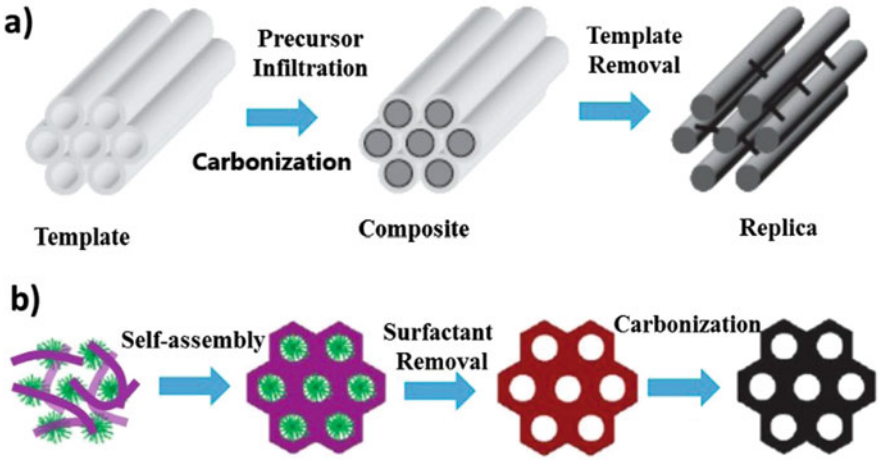

Fig. 5.5 Schematic comparing (**a**) hard template-based and (**b**) soft template-based synthesis strategies. Reproduced with permission from Ref. [64], Copyright Royal Society of Chemistry, 2017

pore diameters, particle morphologies, and framework microstructures are currently available. Typically, the methods of OMC synthesis can be broadly categorized into two: (1) hard-templating (impregnation and etching back) and (2) soft-templating (direct synthesis) as shown in Fig. 5.5a and b, respectively [12, 73]. Both these methods involve the formation of mesopores inside the counterpart bulk material [70, 74].

In the hard-templating strategy, mesoporous structures are created using preformed, ordered mesoporous solid template. This method is also called as nanocasting and involves infiltration of the pores of the template with suitable carbon precursor, its carbonization, followed by removal of the template creating mesostructures which are inverse replica of the mold as shown in Fig. 5.5a. It is vital that the employed hard template has 3D pore structure to aid in the formation of porous, interconnected carbon mesostructures after the removal of the template. It is also equally important that the carbonization of the carbon precursor is confined to the mesopores of the template to ensure the formation of replicated carbon structures. This can be achieved by the conversion of the carbon source to a cross-linked polymer before the carbonization process and can be facilitated by acid polymerization catalysts such as sulfuric acid at the surface of the ordered mesoporous template.

The commonly employed hard templates are silica-based ordered mesoporous structures such as MCM, Santa Barbara Amorphous (SBA), and hexagonal mesoporous silica (HMS) series [72, 75]. These templates favor the formation of highly ordered architecture of the mesopores but require stringent acid treatment process for the template removal which results in the loss of ordering of the material at the atomic scale hampering their intrinsic properties. Non-silica-based templates

such as MgO [76] have also been introduced which offer the advantage of the template removal following a milder acid treatment; however, these lack the uniformity of the mesopores as achieved with the silica templates. The carbon precursor also significantly influences the final morphology and properties of the formed OMC [77]. Carbon precursors with loose molecular structures such as sugar, sucrose, and furfuryl alcohol increase the framework shrinkage and result in the formation of higher SSA materials with dominance of micropores in the structural framework [63, 66, 71, 78]. On the other hand, carbon precursors with dense aromatic structures such as pitch, pyrene, polyacrylonitrile, and acenaphthene lead to the formation of replicated OMC with minimum framework shrinkage, high mechanical strength, and negligible microporosity [79–81]. It is noteworthy to mention here that the pore size and symmetric ordering of OMC are dependent on the solid template and not on the interaction between the carbon precursor and the template.

Jun et al. reported OMC designated as CKM-3 using SBA-15 as the template with sucrose as the carbon source and sulfuric acid as the carbonization catalyst [82]. This was the first report on the successful synthesis of OMC with retention of the structural symmetry of the silica template revealing similar diffraction peaks as that of the template. CKM-3 demonstrated similar characteristics as of CKM-1 such as high SSA of about 1500 $m^2\ g^{-1}$ and total pore volume of about 1.3 $cm^3\ g^{-1}$. However, CKM-3 exhibited larger pore size as compared to CKM-1 which is attributed to the thicker pore wall of SBA-15 as compared to MCM-48 template. Another commonly employed hard template is HMS which has a worm-hole structure and the OMCs synthesized with this template consist of interconnected network of carbon "worms" or "nanostrings" [83, 84]. In contrast to SBA-15, HMS is less costly to synthesize and has walls with twice the thickness resulting in the formation of OMCs with larger pore diameter [85, 86]. In the works of Banham et al. [85] and Li et al. [87], OMCs with HMS template were fabricated using sucrose, anthracene, and naphthalene as carbon precursors.

Silica spheres have also been utilized as template for synthesis of OMCs with 3D interconnected mesopores and macropores which have been proved beneficial for efficient mass transport of reactants and products in fuel cell electrochemical reactions. In the work of Lei et al., monodisperse SiO_2 particles with tunable diameter were prepared through the multi-step seed growth using hydrolysis and condensation of tetraethylorthosilicate (TEOS) in aqueous solution of ethanol and ammonia [88]. This resulted in the formation of colloidal solution of silica which acted as seed for subsequent growth of silica particles. The diameter of the silica particles was tuned during the seed growth by additionally injecting 2 ml TEOS into the seed solution at equal intervals of 6 h for total of 8 times. It was found that the diameter of the SiO_2 particles changes from 16.8 nm to 39 nm from first to eighth cycles of seed growth, respectively. The obtained silica particles were pressed into pellets to form the silica template and were mixed with aqueous solution of sucrose and sulfuric acid followed by carbonization at 850 °C in Ar atmosphere. Finally, porous carbon materials were obtained after the removal of the silica template using 20% HF for 12 h. The study revealed that the SSA and mesoporosity of the carbon materials increase with increase in the diameter of the silica particles. Zhang et al. prepared

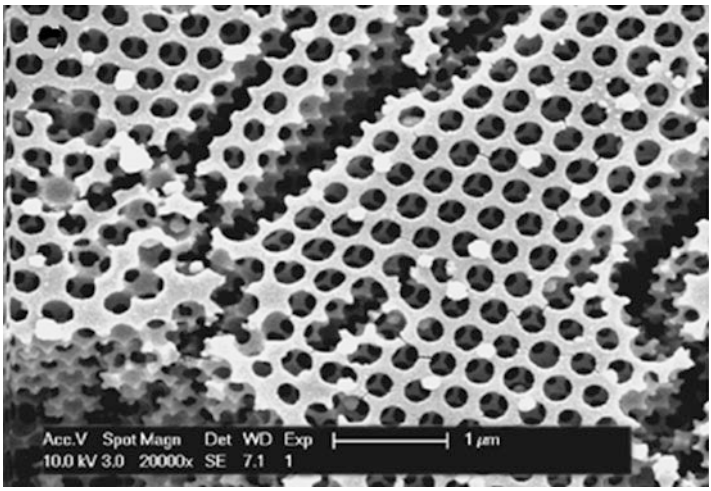

Fig. 5.6 Surface SEM image of hierarchically ordered porous carbon obtained using self-assembly of polymer latex and silica colloid. Reproduced with permission from Ref. [89], Copyright American Chemical Society, 2010

hierarchically ordered porous carbon utilizing silica particles as template through in-situ self-assembly approach of colloidal polymer spheres [89]. The self-assembly strategy of colloidal polymer and silica spheres to prepare hierarchically ordered porous carbons is simple and devoid of any additional infiltration process typical with traditional silica-based templates such as SBA. In this route, both the self-assembly of polymer spheres into the crystal template and the infiltration are completed in-situ in the same system and can be a suitable synthesis route for the mass production of hierarchically ordered porous carbon. In a typical synthesis, colloidal poly(methyl methacrylate-butyl acrylate-acrylic acid) [poly(MMA-BA-AA)] polymer latex (total solid content—15 wt.%) was mixed with colloidal silica, sucrose, and sulfuric acid. The obtained dispersion was solution cast on glass substrate and subjected to complete carbonization at 700 °C in N_2 to yield silica/carbon composite films which were etched using HF solution to form hierarchically ordered porous carbon as shown in Fig. 5.6.

Hollow mesoporous carbon spheres (HMCSs) with hollow core volume and low density are promising candidates for energy applications as compared to OMCs in other morphologies. Li et al. prepared HMCSs using hollow mesoporous aluminosilicate spheres (HMASs) [90]. HMCSs were fabricated through incipient-wetness impregnation method using furfuryl alcohol as the carbon source. The polymerization of furfuryl alcohol was catalyzed in-situ by aluminosilicate template and the final pyrolysis was carried out at 1273 K under N_2 flow. Subsequently, the aluminosilicate template was removed using a 5 wt.% aqueous solution of HF and drying at 373 K overnight to yield HMCSs with SSA of 1809 $m^2\ g^{-1}$ and total pore volume of about 1.01 $cm^3\ g^{-1}$. Gierszal and Jaroniec employed silica colloidal crystals (SCCs) as hard templates for synthesis of hollow core carbon spheres with large pore

volume (6 cm^3 g^{-1}) making them promising candidates for catalytic applications [91]. The porous carbon material was synthesized through incipient-wetness method by impregnating oxalic acid pre-treated SCCs template with solution of resorcinol and crotonaldehyde. The composite sample was subjected to a temperature-controlled polymerization to ensure uniform formation of polymeric film on the silica surface followed by carbonization under N_2 atmosphere at 900 °C for 2 h and removal of the template using diluted HF acid.

The hard-templating method is a highly versatile route for fabrication of OMCs which are negative replicates of the template and hence is widely adopted for construction of a variety of special morphologies such as nanotubes, nanostrings, nanospheres, and nanorods. However, the short-coming is that the various mesostructures are achieved through a chain of tedious multi-step processes at the expense of costly hard templates; thus, making this route incompetent for large scale production. In this regard, soft template synthesis approach comes in handy as instead of etching away the template, OMC can be directly synthesized by self-assembling of block copolymer surfactant and carbon precursor [92].

The soft template route basically involves assembly of carbon precursor and surfactants followed by the removal of the surfactant and subsequent carbonization forming OMCs with defined symmetry and pore size as represented in Fig. 5.5b. In this approach, the interaction between the surfactant and carbon sources drives the self-assembly of the soft template and determines the pore structure of the OMCs [93]. Hence, the direct synthesis route allows an easy adjustment of the structure, shape, and pore size of mesopores through fine tuning of the synthesis conditions such as temperature, ionic strength, pH, type of solvents, and the properties of the template molecules (e.g., hydrophobic/hydrophilic volume ratio) [94–96]. The carbon architectures fabricated through soft template route are more versatile and mechanically stable due to formation of interconnected continuous framework. The soft template route has thus emerged as a simple, flexible, and effective approach for large-scale synthesis of OMCs.

As the name suggests, soft template route employs "soft" molecules such as surfactants and amphiphilic block copolymers for realization of highly structured porous carbon materials [97]. The surfactants or amphiphiles consist of a hydrophilic head group and a hydrophobic tail which on hydrophobic interactions can assemble into discrete spherical, lamellar, or cylindrical structures at concentrations above their critical micelle concentration (CMC). Beyond CMC, these micelles undergo self-organization and aggregate to form diverse mesostructures. The aqueous surfactant assembly approach results in highly ordered mesostructures with well-controlled morphologies and tailored pore sizes. Utilizing this strategy, Zhang et al. prepared tailored mesostructured OMCs (FDU-16, FDU-15 and FDU-14) through organic–organic assembly of resols and triblock polymers [98]. In their work, phenol/formaldehyde resin was used as carbon precursor; whereas, Pluronic F127 and Pluronic P123 were used as triblock copolymer templates for the fabrication of FDU-16 and FDU-14, respectively. For the synthesis of FDU-15, an additional hydrocarbon was employed as swelling agent. The authors also demonstrated the usage of hydrocarbons (hexadecane and decane) to tune the pore size

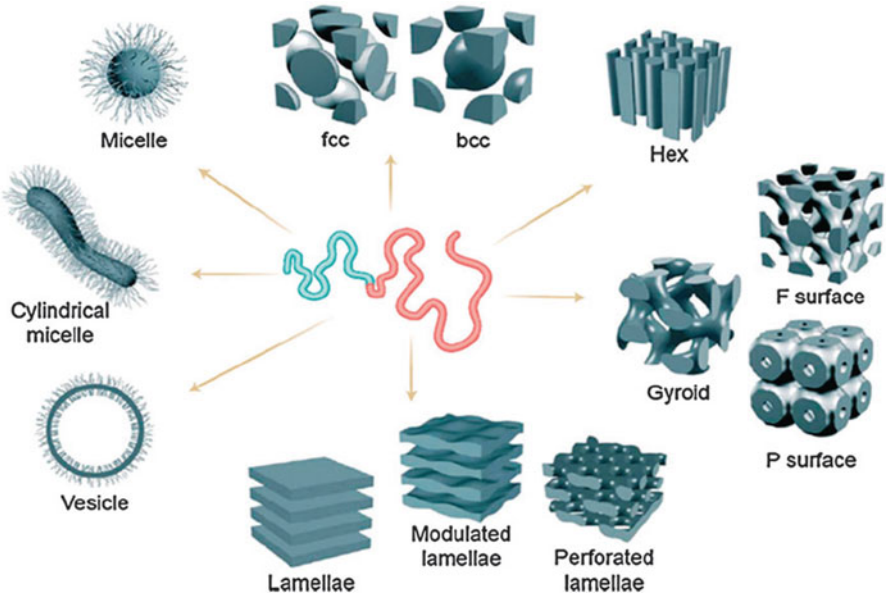

Fig. 5.7 Schematic representation of the various morphologies formed by block copolymers. Reproduced with permission from Ref. [74], Copyright Royal Society of Chemistry, 2012

(4.1–6.8 nm) of OMCs. Using a similar approach, Meng et al. tuned the mesostructures of OMCs from 2D hexagonal to 3D caged cubic and lamellar frameworks by modulating the mass ratio of the polymer precursors (resol) and amphiphilic Pluronic surfactants [99]. The Pluronic copolymers, particularly the triblock copolymers poly(ethylene oxide)-*b*-poly(propylene oxide)-*b*-poly(ethylene oxide) (PEO–PPO–PEO) (e.g., P123, F127, and F108), have been extensively utilized for the synthesis of OMCs with variable mesostructures. The success of this family of block polymers in achieving complex morphologies (Fig. 5.7) and tunable pore architectures is attributed to the microphase separation behavior of block copolymers facilitated by the opposite long-range repulsive and short-range attractive forces prevalent in the constituent blocks [100, 101].

Another commonly employed soft template strategy to prepare OMC materials is evaporation induced self-assembly (EISA) method. EISA approach involves the co-operative self-assembly of the templating agent and organic precursor through the evaporation of the solvent. It is a facile method and can be easily fine-tuned by adjusting synthesis conditions such as acidity of the reaction solution, surfactant, and phenol/template ratio [97, 102–104]. In the pioneering work of Meng et al., highly ordered mesoporous carbon frameworks were prepared using EISA method through organic–organic assembly of PEO-PPO-PEO triblock copolymers (Pluronic P123, F127, and F108) and resols (phenol-formaldehyde) with ethanol as the solvent [105]. They demonstrated synthesis of OMCs with diverse mesostructures such as hexagonal (FDU-16), cubic (FDU-15), bi-continuous cubic (FDU-14), and lamellar

by controlling the ratio of phenol/template and the PEO/PPO segment in triblock copolymer. The evaporation of ethanol assisted in the assembly of the organic precursor and template mainly through hydrogen bonding. Following a similar approach, Wang et al. prepared a functional composite of OMC/tungsten carbide (OMC/WC) with 2D hexagonal mesostructures using Pluronic F127 as a soft template, ammonium metatungstate as tungsten precursor, and phenol/formaldehyde resol as the carbon source through ethanol assisted evaporation [106]. In the works of Zhao et al., by employing ethanol assisted EISA strategy, OMC FDU-15 with different pore sizes (4.0–8.1 nm) was prepared using pore expanding agents, TEOS and decane [107]. This synthesis also utilized Pluronic F127 as a soft template and phenol/formaldehyde as the carbon source.

OMCs with large pores are highly desired as they offer the possibility of efficient loading of catalyst NPs without blocking the pore channels. It is well known that the hydrophobic volume of the template determines the pore size. Hence, block copolymers with long hydrophobic chains are promising candidates for fabrication of mesostructures with large pores. In this regard, Pluronic copolymers have restricted application due to limited short hydrophobic PPO blocks which lead to formation of mesoporous materials with pore size less than 12 nm without using any pore expanding agents such as 1,3,5-trimethylbenzene (TMB) [108, 109]. Another disadvantage associated with Pluronic family of block polymers is their low-temperature degradation (200–350 °C) even in inert atmosphere which gives rise to amorphous or semi-crystalline mesoporous structures. Considering these aspects, non-Pluronic copolymers such as poly(ethylene oxide)-*b*-polystyrene (PEO-*b*-PS), poly(2-vinylpyridine)-poly(isoprene) (P2VP-PI) and poly (4-vinylpyridine)-polystyrene(P4VP-PS) are adopted as promising templates to synthesize crystalline OMCs driven by strong hydrogen bonding interaction between the carbon precursor and the template [110]. These synthetic templates have longer rigid hydrophobic segments, higher carbon content, and stability as compared to their Pluronic counterparts. However, different from PEO-PPO-PEO block copolymers, non-Pluronic block copolymers have high molecular weight and hydrophobic segments which make them insoluble in water, and even with ethanol. Hence, synthesis of mesostructured materials using non-Pluronic copolymers as templates is mostly limited through the EISA approach [74, 97, 111, 112].

Comparing the hard template and soft template routes for preparation of OMCs, each has its own advantages and limitations [64, 97, 113]. Following hard template strategy, it is easier to obtain highly crystalline and graphitized OMCs; whereas, amorphous or semi-crystalline OMCs are obtained through soft template route. Also, soft template route offers a low cost, simple, and convenient methodology suitable for mass production of OMCs, while hard template approach is relatively complex, expensive, and time consuming, making it unsuitable for large-scale industrial production.

5.3.2 Surface Functionalization of OMCs

OMCs exhibit unique architectures and properties such as interconnected mesoporous structures, narrow pore size distribution, and high surface area which are highly desirable for application as support materials. However, the effective dispersion/anchoring of metal NPs into the mesoporous voids through the commonly employed "wet chemistry" approach is limited by the poor compatibility of hydrophobic carbon and hydrophilic solvents employed to dissolve the metal precursors [78, 114]. Hence, in order to achieve uniform and efficient dispersion of metal NPs, it is imperative to modify or functionalize the surface of OMCs with specific moieties, affinities, and reactivity [115, 116]. The surface modification or functionalization of OMCs renders surface functional groups which act as anchoring sites for metal catalysts and also aids in metal–support interaction which favorably enhances the activity and durability of the catalysts.

Surface functionalization of porous materials can be effectively achieved through introduction of oxygen-containing functional groups such as carboxylic, anhydride, phenolic, and carbonyl, which enhances the surface hydrophilicity of the carbon support aiding its dispersion in various solvents. Out of these, acid treatment is demonstrated to be an effective way of functionalization which makes the surface of carbon support act as site for metal catalysts and assist their anchoring. In the works of Guha et al. [117] and Salgado et al. [118], the surface of OMC support was modified using HNO_3 and the studies demonstrated strong dependence of the extent of functionalization on the catalytic activity of the supported metal electrocatalysts. However, the enhanced dispersibility of acid modified OMCs occurs at the expense of electrical conductivity and mechanical strength. In such a scenario, it is important to carefully select the acidic oxidation conditions such as type of oxidant, temperature, and treatment duration, since excessive oxidation leads to structural disintegration and subsequent dissolution of the carbon.

Surface modification of OMCs using heteroatoms such as nitrogen and sulfur has also been reported as an effective approach to tune their catalytic activity and stability. Perini et al. prepared nitrogen modified porous carbons using sucrose and ammonia as carbon and nitrogen source, respectively [119]. The study showed the effect of nitrogen defects on metal–support interactions and revealed that the nitrogen functional groups controlled the dimension and the dispersion of metal catalysts. In the work of Xiao et al., surface modification of CMK-3 with nitrogen doped carbon using polydopamine as the nitrogen source was attempted [120]. The results demonstrated formation of three phase interface areas with nitrogen modification of CMK-3 and higher electrochemical performance. Ji et al. utilized sulfur modified OMC which acted as metal trap because of its strong affinity towards noble metals due to soft acid–soft base interaction; this helped the effective dispersion of the catalyst particles [121]. Pt-based intermetallic nanocrystallites with sizes as low as 1.5 nm, which can be tuned up to ~3.5 nm, were formed with surface sulfur modified OMC supports.

Surface functionalization of OMCs can also be effectively achieved through charged species which assist in the improvement of synergistic interactions between metal catalysts and modified OMC supports. With positively charged cetyltrimethylammonium bromide (CTAB) surfactant, Zhou et al. modified the surface of OMC materials as support for Pt-NPs and demonstrated improvement in the wettability of OMCs with addition of CTAB resulting in better dispersion of Pt-NPs [122]. Li et al. functionalized OMCs with sodium dodecyl sulfate (SDS) followed by in-situ deposition of Pd NPs through MW assisted route. The electrostatic interaction between negatively charged SDS and positively charged Pd^{2+} facilitated the facile formation of the functional composite materials [123]. In the work of Zhang et al., positively charged, polyelectrolyte poly-(diallyldimethylammonium chloride) was used to wrap the OMCs which aided in facile anchorage of Pt-NPs through electrostatic interactions [124].

5.3.3 Application of OMCs as Support for Metal Catalysts

For the application as metal catalyst support for fuel cell, OMC materials offer several advantages compared to the traditional carbonaceous materials such as CB. Both OMC and CB support materials have high SSA to load the metal catalyst NPs and effectively reduce the expensive noble metal content. However, in the case of CB, metal particles get buried in the micropores making them inaccessible by the reactant fuels resulting in lower catalytic activity. In contrast, the mesoporous structure of OMCs effectively aids in mass transport of reactants and increases metal particle utilization thereby enhancing the mass activity of the catalysts. OMCs also exhibit higher chemical stability as compared to CBs. Furthermore, the structure, morphology, and physicochemical properties of OMCs can be easily customized by adjusting the synthesis conditions, template, type, and amount of carbon precursor and incorporation of heteroatoms.

Momčilović et al. employed OMC prepared through EISA method using resorcinol as the carbon precursor and Pluronic F127 as the soft template with ethanol/water as the solvent, as Pt catalyst support for HOR and ORR in acidic medium [125]. The kinetics of HOR and ORR on OMC supported Pt catalyst (Pt–OMC-SAM-800/3) was investigated using rotating disk electrode (RDE) voltammetry and the results showed reversible HOR kinetics and comparable ORR catalytic activity of Pt–OMC-SAM-800/3 with that of traditional carbon supported Pt electrocatalysts. Higher ORR and MOR catalytic activity was reported by Cao et al. with mesoporous carbon (MC) supported Pt catalysts as compared to Pt/XC72R and commercial Pt/C catalysts [126]. The improved electrocatalytic performance with Pt/MC was ascribed to the unique mesoporous structure of MCs and enhanced interaction between Pt-NPs and MCs. In the work of Xu et al., higher MOR and ORR activities along with stability were reported for Pt-NPs supported on ordered mesoporous carbon sphere (OMCS) array than Pt/CB and commercial Pt/C catalyst [127]. The enhanced performance of Pt/OMCS was attributed to the unique hierarchical structure of

OMCs supports with ordered macropores and mesopores which facilitated the mass transport of fuels and improved the dispersion of Pt particles. Joo et al. studied the effect of particle size of Pt-NPs supported on OMC on ORR and MOR activity [128]. Through a modified, sequential impregnation-reduction method, controlled Pt size from 2.7 to 6.7 nm was achieved. The study revealed volcano-type mass activity curve exhibiting the maximum activity at the Pt size of 3.3 nm for both ORR and MOR. In another work, Joo et al. investigated the effect of particle size of OMC support for Pt catalyst on ORR in DMFC [129]. They employed OMC with particle sizes of 100 nm, 300 nm, and 700 nm (OMC-100, OMC-300, and OMC-700) and deposited Pt-NPs of ~3 nm onto the supports. The electrochemical results revealed no significant influence of OMC particle size on ORR activity of the Pt/OMC catalysts. All the three catalysts exhibited similar catalyst utilization efficiency and ORR electrocatalytic activity.

Ahn et al. carried out studies to optimize the ionomer content in OMC supported Pt catalyst to achieve better PEMFC performance [130]. Electrodes with different ionomer content in the range of 5–30 wt.% were prepared as cathode and fabricated into MEA (MEA-5, MEA-10, MEA-15, MEA-20, and MEA-30) to assess their performance. The polarization curves with the fabricated MEA showed higher potential in the low current density region with increase in ionomer content due to their ability to form three phase boundaries. However, too much ionomer as in the case of MEA-30 resulted in poor performance due to strong hydrophilic interactions between H_2O and ionomer, restricting mass transport of reactants as well as the product, water. On the contrary, at higher current density, MEA with lower ionomer content demonstrated higher performance due to facile mass transport of product H_2O produced by electrochemical reactions. With Pt/OMCs as cathode catalysts for PEMFC, the highest ESA, Pt utilization, and cell voltage at high current density were obtained with MEA-10 containing 10 wt.% ionomer. Kim et al. studied the influence of three types of OMCs with different frameworks (CMK-3, CMK-3G, and CMK-5) as support materials for Pt on the ORR activity and durability [131]. These OMC materials were prepared using the same hard template SBA-15 and had similar hexagonal mesostructures, but with different carbon framework structures and degree of graphitization which significantly influenced their surface area, microporosity, and electrical conductivity. The authors showed a direct dependence of micropore volume of OMC supports to their catalytic activity and durability. The highest ORR activity was achieved with Pt/CMK-3G catalyst, and it was ascribed to the formation of crystalline Pt-NPs on the highly graphitic, crystalline CMK-3G framework which resulted in weaker adsorption of surface oxide and stronger interaction between the Pt particles and the support.

Surface functionalized OMC through nitric acid oxidative treatment was used as Pt catalyst support for DMFC by Calvillo et al. [132]. The introduced oxygen functional groups assisted in uniform dispersion of Pt particles and showed better MOR catalytic activity as compared to commercial Pt/C catalyst. Morales-Acosta et al. compared the influence of OMC, MWCNT, and Vulcan support materials on methanol, ethanol, and ethylene glycol electro-oxidation reaction (MOR, EOR, and EGOR, respectively) activity in direct alcohol fuel cells (DAFCs) [133]. The support

materials were pre-treated with HNO_3/H_2SO_4 solution before depositing Pt catalysts to modify their surface with oxygen-containing groups. It was found that the use of OMC enhances the catalytic activity towards the three reactions. It also exhibited higher electrochemical stability than the other two supports showing ESA loss of only 12% after 500 cycles of accelerated durability test (ADT). Samiee et al. proposed in-situ functionalization of OMC (CMK-3) with MWCNT following a two-step method [134]. In the first step, mesoporous carbon was functionalized with NiO following an impregnation route using the solution of nickelocene ($NiC_{10}H_{10}$) in ethanol. Subsequently, the Ni functionalized OMCs were utilized as substrate for deposition of MWCNT through CVD technique. It was found that the functionalization of CMK-3 with MWCNT resulted in partial damage of the mesoporous structure of OMCs; however, CMK-3 CNT supported Pt catalyst (CMK-3CNT20Pt) exhibited superior ORR catalytic activity and fuel cell performance compared to the industrial, 40 wt.% Pt/Vulcan catalyst.

Nsabimana et al. investigated the influence of boron-doped OMC support for Pt (Pt–BOMC) on MOR catalytic activity and compared the performance with undoped OMC supported Pt (Pt–OMC) and commercial Pt–C catalysts [135]. Pt–BOMC exhibited remarkably higher MOR catalytic activity than that of Pt–OMC and Pt–C catalysts; this was attributed to stronger Pt–support interactions attained with boron doping. Song et al. employed phosphorous doped OMCs supported Pt as anode catalyst in DMFC [136]. The study showed that addition of P enhances oxygen content of the support facilitating uniform dispersion of Pt-NPs with particle size of 3.5 ± 0.4 nm leading to higher ESA. Pt-based bi-metallic NPs have also been supported on OMCs and employed as catalyst materials in low-temperature fuel cells. Bruno et al. showed 15% higher peak power density with Pt–Ru/OMC anode catalyst over Vulcan supported catalyst, Pt–Ru/C [137]. Hung et al. synthesized core-shell Pt–M (M = Ru, Fe, and Mo) supported on OMCs and investigated them as anode catalyst for MOR in DMFC [138]. The bimetallic Pt–M NPs were well dispersed in the pore channels of the OMC support and showed superior MOR catalytic performance with remarkable tolerance to CO poisoning as compared to typical commercial PtRu/Vulcan XC72 anode catalyst.

5.4 Green Carbons

Carbon materials have made momentous impact in energy storage and conversion applications. Advanced functional carbonaceous materials are still being explored to achieve sustainable energy in the form of electrochemical power sources. Particularly, in low-temperature fuel cells, carbon materials play a vital role as supports and effectively assist in fuel cell catalysis as discussed in the previous sections. It is to be noted that preparation of most of carbonaceous supports such as graphene, carbon nanotubes (CNTs), carbon nanofibers (CNFs), CB, and activated carbons which are typically employed as catalyst supports involves tedious synthesis procedures, complicated apparatus, usage of metal catalysts, high temperature processing and

are most often derived from expensive fossil fuel-based precursors making them undesirable for sustainable energy production [139–143]. In such a scenario, the realization of sustainable energy through application of these carbonaceous materials in fuel cells sounds "misnomer." Hence, the development of "green carbon" through environmentally benign and economically sustainable way gains utmost significance and urgency for their applications in fuel cells. Considering these aspects, this section discusses biomass derived novel carbons as viable support materials for fuel cell catalysts. The methodology involved in anchoring of diverse NPs onto these "green carbon" is also discussed at the end of this section for better understanding of the overall process involved in the preparation of "green carbon"-based catalysts for low-temperature fuel cells.

5.4.1 Biomass as Source of Novel Carbons

Mother Nature provides limitless renewable biomass source which can be effectively converted to valuable "green carbon" through viable, environmentally and economically sustainable approaches. Biomass sources are readily available, accessible, and recyclable across planet Earth. They also offer a wide variety and structural diversity for fabrication of novel carbons with fine-tuned chemical structure and morphology for the targeted application.

Plants (lignocelluloses) are one of the most common and readily available sources of biomass. Lignocellulose is the main structural constituent of the cell walls in woody and non-woody plants. They are composed of cellulose, hemicellulose, and lignin which act as source of carbon. Glucose, the building block of cellulose, is a cheap and facile source of carbon. Using glucose as carbon precursor, Falco et al. prepared functionalized carbon materials through hydrothermal carbonization (HTC) [144]. The authors showed significant influence of processing temperature and time on glucose derived carbon particle diameter and size distribution. They also showed that, through proper control of processing conditions, the final chemical structure of carbon can also be tuned from oxygen rich carbonaceous polyfuran to carbonaceous network with extensive aromatic domains. Using borax (sodium borate) mediated hydrothermal approach with glucose as carbon source, Fellinger et al. prepared hierarchically structured carbon aerogels [145]. The experimental results demonstrated that the sugar:borax ratio controlled the primary carbon NP size; whereas, their spinodal destabilization resulted in the controlled aggregation of carbonaceous particles leading to the formation of monoliths. Liu et al. prepared porous carbon structures and carbon sheets with glucose precursor through molten salt process using different oxysalts ($KNmO_x$; Nm = H, B, C, N, P, S, Cl), dissolved in the LiCl/KCl solvent [146]. The type of oxysalt employed significantly influenced the morphology, surface area, microporosity, and pore volume of the resultant carbons.

Sucrose is another naturally renewable bio-resource and is effectively utilized for sustainable generation of advanced functional materials. Sucrose has been the most

popular carbon precursor for fabrication of OMCs. Xiao et al. fabricated OMCs with selective morphologies using SBA-15 and sucrose as template and carbon precursor, respectively, by simply controlling the infiltration processing conditions [147]. Ting et al. synthesized OMCs with hexagonal mesostructures through organic–inorganic self-assembly of sucrose, Pluronic P127 and TEOS in acidic conditions [148]. The structural properties of the developed high surface area carbon materials (1225 $m^2\ g^{-1}$) were tailored by adjusting the reaction parameters and compositions. Sivadas et al. prepared nitrogen enriched mesoporous carbon through simple heating and KOH activation process utilizing sucrose (carbon source) and urea (nitrogen source) [149]. By adjusting the amount of sucrose, carbon, and KOH, mesoporous carbons with different N content were prepared with high SSA and pore volume. Hierarchically porous carbon monoliths with SSA and pore volume up to 1426 $m^2\ g^{-1}$ and 3.097 $cm^3\ g^{-1}$, respectively, were also prepared by Yu et al. using sucrose and amino-functionalized monolithic NH_2–SiO_2 through hydrothermal nanocasting strategy [150]. Yu et al. prepared biomass derived carbon materials through HTC of carbohydrate precursors (xylose, glucose, sucrose, and starch) and concluded that the porosity of the developed carbon functional materials was highly dependent on thermal treatment temperature [151].

Cellulose derivatives are also promising raw materials for preparing carbonaceous materials due to their naturally ubiquitous abundance, inherent non-toxicity, and 1D nanostructures [152, 153]. Celluloses are comprised of only C, H, and O atom; hence, co-doping with one or more heteroatoms is generally carried out to achieve carbon materials with superior properties. N-doped carbon nanosheets with high SSA (~1362.36 $m^2\ g^{-1}$) and large pore volume (~3.36 $cm^3\ g^{-1}$) were prepared by direct pyrolysis of cellulose/urea [154]. 3D porous networked Fe and P co-doped CNFs with large surface area were derived by carbonizing bacterial cellulose (BC) [155]. Similarly, by direct pyrolysis and subsequent ammonia activation of BC, networked nitrogen doped CNF aerogel was fabricated with high density of N-containing active sites (5.8 at.%) and high SSA (916 $m^2\ g^{-1}$) [156]. Lai et al. also prepared nitrogen doped CNF network by a single step carbonization process; here the BCs were coated with polyaniline as the nitrogen source to produce 3D porous network [157]. Mulyadi et al. prepared hybrid 3D carbon nanomaterials, N,P-doped carbon with N,S-doped CNF using cellulose nanofibril precursors [158]. High surface area carbon aerogels with interconnected nanostructures were also prepared using BC pellicles as biomass source [159, 160]. Sun et al. prepared networked carbonaceous nanofibers through direct pyrolysis of BC pellicles under nitrogen atmosphere [161]. Using 3D nanostructured BC pellicles as biomass precursor, Wu et al. fabricated a highly electrochemically active nanocomposities of Mo_2C NPs embedded within BC derived carbonaceous framework [162].

Chitosan (CS) is the second most naturally abundant nitrogen-containing biopolymer after cellulose and has been successfully employed as biomass precursor for realizing advanced functional carbonaceous materials. Rybarczyk et al. prepared highly porous activated carbon material by pyrolysis of chitosan with $ZnCl_2$/LiCl salt mixture [163]. The resulting CS derived carbon materials showed SSA of

1317.97 $m^2 g^{-1}$ with total nitrogen content of 6.5%. Nitrogen enriched (ca. 6–7 wt. %) micro/mesoporous activated carbon materials were prepared by Kucinska et al. utilizing CS and $ZnCl_2$ as activating agent via oxygen-free carbonization [164]. The surface area, pore volume, and pore size distribution of the carbons were tailored by tuning the CS–$ZnCl_2$ ratio in the precursor. Following a similar $ZnCl_2$ assisted carbonization and activation process, Wang et al. also prepared hierarchical macro/microporous N-doped carbon materials with large surface area [165]. Jiang et al. produced N-doped porous carbon materials through a simple template carbonization process using carboxymethyl chitosan and $Zn(NO_3)_2 \cdot 6H_2O$ as the carbon/nitrogen source and template, respectively. The effect of two direct synthesis methods, *viz.* solution-phase and solid-phase, on physicochemical properties of the obtained carbon materials was thoroughly investigated in a study which demonstrated formation of N-doped (2.06 at.%) porous carbons with higher surface area (1956 $m^2 g^{-1}$) and larger pore volume (1.48 $cm^3 g^{-1}$) with solution-phase method.

Novel carbonaceous materials can also be prepared using green plants as carbon precursors. Chen et al. prepared N-doped nanoporous carbon nanosheets (NCS) using a wetland plant, cattail through a facile hydrothermal treatment and subsequent post-treatment in ammonia gas [166]. The prepared NCS materials exhibited microporous structure with high surface area (898 $m^2 g^{-1}$) and high content of nitrogen (9.1 at.%). Liu et al. obtained nitrogen self-doped porous carbon through simple pyrolysis of water hyacinth at controlled temperatures (600–800 °C) with $ZnCl_2$ as an activation reagent [167]. The obtained porous carbon showed surface area up to 1199.3 $m^2 g^{-1}$ and nitrogen content of 5.02 at.%. It was found that different forms of nitrogen (pyridinic, pyrrolic, and graphitic) were incorporated into the carbon molecular skeleton. Through carbonization of natural cotton and subsequent activation with KOH in nitrogen atmosphere, Cheng et al. prepared high surface area carbon aerogel fiber with good electronic conductivity (~860 S m^{-1}) [168]. It was found that depending on the amount of KOH employed during the activation process, the SSA of the carbon aerogel varied from 1536 to 2436 $m^2 g^{-1}$ without any significant change in the electrical conductivity. Using low cost corn husk [169] and mushroom [170] as biomass carbon resource, hierarchically porous carbon was reported through direct pyrolysis and activation process with KOH and H_3PO_4/KOH, respectively.

Animal biomasses are attractive sources for production of functional carbon materials and offer additional advantage of waste management from livestock which are quite challenging. Chicken and pig poultry industries are sources of abundant waste animal biomass. By carbonizing chicken [171] and pig bones [172], high surface area (560–770 $m^2 g^{-1}$) N-doped porous carbon materials were successfully synthesized. Chicken feathers also served as economical and sustainable bio-source for preparation of N,S-co-doped porous carbon materials [173]. Pig skin was used as green source to prepare high surface area (2799 $m^2 g^{-1}$) N-doped porous carbon with $CaCO_3$ as activating agent [174]. Using porcine blood, a series of nitrogen-doped carbon nanospheres were prepared at different pyrolysis temperatures, and it was found that higher percentage of planar N species resulted in excellent electrochemical activity [175]. Fish bio-wastes are considered as excellent

raw materials for preparation of porous nitrogen enriched carbonaceous materials. Wang et al. fabricated porous N-doped carbon material through a simple pyrolysis of fish bone followed by acidic treatment [176]; whereas, Guo et al. prepared N-doped porous carbon network by fish-scale pyrolysis and subsequent activation by $ZnCl_2$ [177]. Eggs are natural biological materials rich with protein and cholesterols. Furthermore, they are also cheap source of heteroatoms such as N, S, and P alleviating the need of external doping agents making them suitable alternative carbon precursors to obtain in-situ heteroatom doped porous carbon materials. Egg derived heteroatom doped mesoporous carbons with large surface area and high pore volume have been reported through spray drying process [178] and carbonization with graphical carbon nitride which acted as template, N source, and swelling agent [179]. Heteroatom doped mesoporous carbons were also prepared by a single step facile pyrolyzing process [180]. Apart from the poultry-based bio-waste, human hairs are another widely available organic waste and being rich in heteroatoms (N,S) can serve as low cost scrap materials to fabricate valuable porous carbon materials. N,S co-doped porous carbon materials with large surface area and high porosity were developed through a simple approach comprised of degradation of human hair followed by carbonization and subsequent activation/graphitization process [181–183].

5.4.2 New Family of Green Carbon Supports

Biomass derived advanced "green carbon" materials typically have a large surface area with beneficial porous structures which facilitate efficient mass transportation of reactants and products [184, 185]. Furthermore, many biomass precursors contain abundant heteroatoms, which can directly serve as doping agents to create catalytically active sites [186, 187]. Also, the conductive carbon framework can enable the efficient electron transfer for electrochemical reactions. Hence, biomass derived green carbons are promising support materials for low-temperature fuel cell catalysts. In the work of Zhou et al., nitrogen containing mesoporous carbon (CS) with high surface area (516.6 $m^2\ g^{-1}$) and total pore volume (0.45 $cm^3\ g^{-1}$) was derived from carbonizing soybeans [188]. CS was employed as support for Pt-NPs for electro-oxidation of methanol and the catalytic performance was compared with Pt supported on Vulcan carbon XC-72. Compared with traditional carbon support, Pt/CS showed higher methanol oxidation onset potential and 1.5 times higher peak oxidation current (Fig. 5.8a) along with higher durability as shown by chronoamperometric results (Fig. 5.8b). The enhanced performance of Pt/CS was ascribed to more active sites for methanol oxidation with CS supports as compared to Vulcan XC-72 and unique dendritic morphology of Pt-NPs. In another work of Zhang et al., okara-derived carbon (ODC) was prepared by carbonizing okara at 800 °C under N_2 atmosphere and was employed as support for Pt-NPs for MOR [189]. The electrochemical results revealed higher electrocatalytic activity and resistance to CO poisoning of Pt/ODC than Pt/C catalyst. This improved MOR electrocatalytic performance of Pt/ODC was attributed to the high degree of

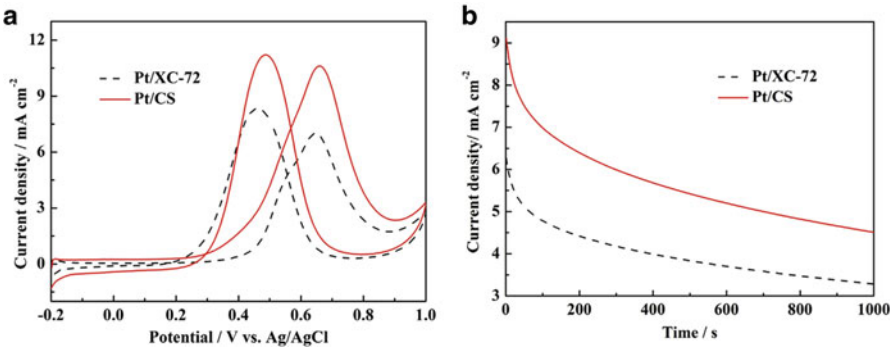

Fig. 5.8 (**a**) CV plots at scan rate of 50 mV $s^{-1}$and (**b**) chronoamperometric curves of Pt/CS and Pt/XC-72 electrodes in N_2-saturated 0.5 mol L^{-1} H_2SO_4 + 0.5 mol L^{-1} CH_3OH. Reproduced with permission from Ref. [188], Copyright Elsevier, 2014

graphitization and multi-grain interfaces with ODC supports which are conducive for favorable formation of more catalytically active sites. Pt-NPs supported on chitosan-carbon black derived N-doped carbon material (Pt/NC) were investigated for MOR and the performance was compared with commercial Pt/C and home-made Pt/C catalysts [190]. Pt/NC demonstrated better MOR electrocatalytic activity and stability than the commercial catalysts which was attributed to synergistic metal–support interactions.

Yan et al. explored mesoporous bowl-like carbons (BLCs) as support for Pt-NPs [191]. BLCs were prepared using glucose as carbon source and solid core mesoporous shell silica spheres as template. A regular bowl shaped mesoporous structured carbon as shown in Fig. 5.9 was obtained after the etching process with HF. The derived mesostructured carbons exhibited high surface area (1108.3 m^2 g^{-1}) and large pore volume (2.7 cm^3 g^{-1}) which are highly desirable for uniform and stable dispersion of Pt-NPs. Moreover, the mesopores of BLCs assist in mass transfer of reactants and products during catalytic reactions. BLC supported Pt catalyst (Pt/BNC) were evaluated for MOR and ORR activity. For a meaningful comparison, MOR and ORR activity of commercial Pt/C (TKK) was also evaluated. Pt/BLC demonstrated 2.6 times (1846 mA mg_{Pt}^{-1} *vs.* 723 mA mg_{Pt}^{-1}) and 1.6 times (180.6 mA mg_{Pt}^{-1} *vs.* 114.2 mA mg_{Pt}^{-1}) higher catalytic activity for methanol oxidation and oxygen reduction, respectively, than that of TKK. Furthermore, Pt/BLC also exhibited higher stability for ORR and lost only 6.9% of its catalytic activity in contrast to 18.9% loss by TKK catalyst after 10,000 potential cycles which was ascribed to stable attachment of Pt-NPs on mesoporous BLC support and consequent stronger force of physical interaction. Using soluble sucrose as precursor, ultrathin carbon layer (UTCL) stabilized Pt-NPs were reported by Cheng et al. [192]. The starch stabilized Pt-NPs in the colloidal state were further supported on Vulcan XC-72R carbon followed by pyrolysis at 350 °C for 10 min under Ar atmosphere forming UTCL (≈0.58 nm) around Pt-NPs. Thus fabricated Pt/UTCL-C catalyst displayed comparable ORR activity (mass activity, 112.5 A g^{-1} vs. 116.2 A g^{-1})

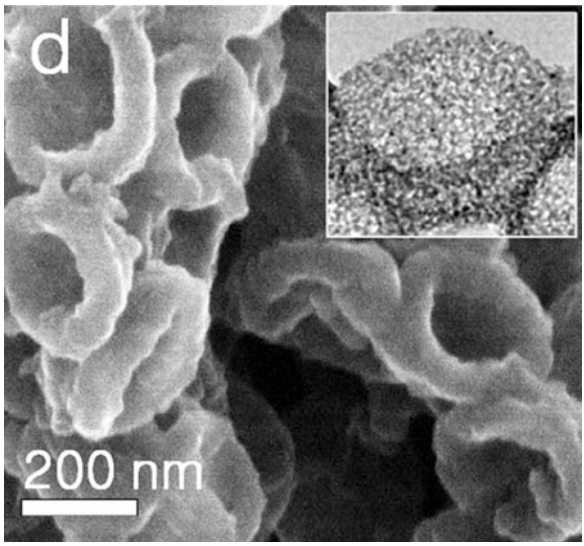

Fig. 5.9 SEM image of the BLCs showing regular bowl shape. Inset shows TEM images showing mesoporous structure of BLCs. Reproduced with permission from Ref. [191], Copyright Elsevier, 2013

as of commercial Pt/C which was also heat treated in an identical manner. However, Pt/UTCL-C catalyst demonstrated excellent stability with 40% loss of mass activity after 10,000 cycles of accelerated electrochemical aging tests as compared to 69% loss shown by conventional Pt/C catalyst. The superior stability of the former catalyst was attributed to UTCL around the catalyst particles that hindered migration and agglomeration of Pt-NPs and their detachment from the support. Liu et al. used pig bone derived hierarchical porous carbon (HPC) as support material for Pt electrocatalysts [193]. HPCs were prepared by carbonizing, activation by KOH, and acid treatment of the pig bones. The resulting nitrogen self-doped HPC exhibited high surface area (2157 $m^2\ g^{-1}$) with three-dimensional open macropore structure. HPC supported Pt exhibited larger ESA (Pt/HPC = 117.3 $m^2\ g^{-1}$) than that of carbon black supported Pt-NP catalyst (Pt/Vulcan XC-72 = 66.7 $m^2\ g^{-1}$), suggesting higher Pt utilization by the former catalyst owing to their open macroporous structure and nitrogen atoms. Compared with Pt/Vulcan XC-72, Pt/HPC also displayed higher ORR catalytic activity and stability. The enhanced performance was attributed to hierarchical porous structures, large surface area, and large amount of micropores and nitrogen-doped surface state of HPC which facilitated the mass transportation and improved the catalytic activity of Pt-NPs.

5.4.3 Anchorage of Nanoparticles on Green Carbons

In contrast to conventional CB support materials, biomass derived mesoporous carbon materials are fabricated through low cost routes utilizing renewable resources and also offer added advantage of uniform and stable dispersion of metal NPs by

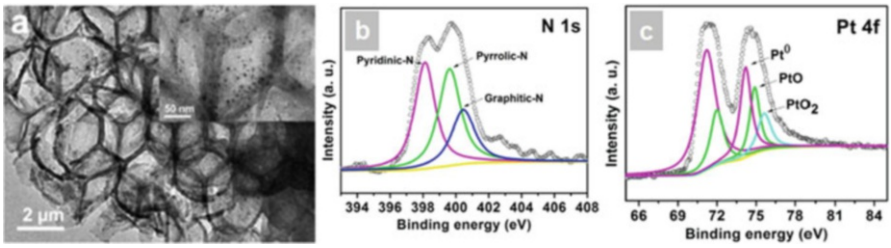

Fig. 5.10 (**a**) TEM images, (**b**) XPS N 1s spectra, and (**c**) XPS Pt 4f spectra of Pt-N/C PMCs. Reproduced with permission from Ref. [194], Copyright Elsevier, 2017

virtue of self-doped heteroatoms which create anchoring sites for deposition of NPs. Hence, biomass derived mesostructured porous carbon supported Pt-based catalysts exhibit improved electrocatalytic activity and stability than conventional Pt/C catalyst.

Cheng et al. used 3D N-doped porous microspherical cavities derived from self-polymerization of polydopamine (PDA) and polystyrene microspheres (PS) as support materials [194]. Pt-NPs were decorated onto the mesoporous support through in-situ reduction of Pt precursor (K_2PtCl_6) on the surface of PDA followed by carbonization process. Pt-NPs with average diameter of 1.9 ± 0.5 nm were deposited onto the support Fig. 5.10a) and the catalyst showed high percentage of metallic Pt, pyridinic N (39.2%), and graphitic N (22.6%) in the resulting Pt–N/C catalysts as shown by XPS results (Fig. 5.10b, c). The electrochemical results proved enhanced ORR catalytic activity, stability of Pt–N/C PMCs, and remarkable methanol tolerance as compared to Pt/C catalysts. The improved electrocatalytic performance was attributed to the combined effect of higher content of metallic Pt (Pt^0), active pyridinic and graphitic along with the porous structure of the support that facilitated mass transport of reactant and electrolyte to the active sites. In the work of Wang et al., hard carbon spherules (HCS) derived from hydrothermal carbonization of sugar were used as support [195]. Pt-NPs were deposited onto the support following two reduction methods involving reduction of the Pt precursor with $Na_2S_2O_4$ in aqueous solution (Pt/HCS1) or EG (Pt/HCS2). It was found that reduction conditions of Pt precursor influenced the size and aggregation of the Pt particles and subsequently their catalytic activity. High and well-dispersed Pt-NPs with average diameter of 5 nm were obtained with EG reduction method. Pt/HCS2 also exhibited 9.5 times higher electrocatalytic activity than Pt/Vulcan XC-72 catalyst which was attributed to uniform dispersion of the Pt-NPs and better electrode–electrolyte contact. Fe-doped porous graphitic carbon nanostructure (GCN) derived from filter paper was used as Pt support by Afraz et al. [196]. Pt-NPs were electrochemically deposited onto glassy carbon electrode modified with GCN support (Pt–NP/GCN) through potentiostatic double-pulse technique using 0.5 mM H_2PtCl_6 in de-aerated KNO_3 solution. Pt–NP/GCN displayed higher methanol oxidation current density than commercial Pt/C electrode. The improved electrocatalytic performance was attributed to synergistic metal–support interaction and iron oxide impurity of GCNs.

Biomass derived support materials for Pt were also prepared by pyrolyzing silkworm cocoon with ferric chloride as activator [197]. Thus, obtained cocoon-derived activated carbon (AC) with high surface area (756 $m^2\ g^{-1}$) and narrow pore size distribution (3.6 nm). Pt particles were deposited onto the AC support (N–Pt/AC) through hydrothermal route using sodium citrate and ethylene glycol. N–Pt/AC demonstrated higher activity towards MOR as compared to Pt/C catalyst in terms of higher ESA (98.3 $m^2\ g_{Pt}{}^{-1}$ *vs.* 46.3 $m^2\ g_{Pt}{}^{-1}$) and better CO tolerance. The enhanced performance of N–Pt/AC catalyst was attributed to the multi-grained Pt structure formed as a result of cocoon-derived AC. Lobos et al. utilized biochar produced by pyrolysis of untreated and phosphoric acid treated cellulose as support materials for Cu–Ru@Pt core-shell NPs [198]. The tri-metallic NPs were deposited onto the support through a two-step procedure. Cu–Ru NPs were deposited first onto the carbonaceous materials using $NaBH_4$ reduction of the precursor salts in a weight ratio of 3:1. Finally, the Cu–Ru@Pt core-shell NPs were obtained by galvanic replacement reaction of Cu^{2+} by Pt^{4+} ions. It was found that phosphoric acid treatment modified the carbonaceous support and significantly influenced catalytic activity through surface defect sites (metal–support interaction). Cu–Ru@Pt supported onto the phosphoric acid treated biochar exhibited high ESA and MOR activity with turnover number value of 0.151 mol $site^{-1}\ s^{-1}$ at 0.5 V.

5.5 Conclusions and Outlook

Electrocatalyst support materials significantly influence the performance of low-temperature fuel cells. This chapter briefly discussed the newly developed carbonaceous nanostructures such as graphene, OMCs, and green carbon as alternatives to conventional CB support materials in low-temperature fuel cells. Graphene is a fascinating 2D material and has exceptional properties such as high surface area, high conductivity, and unique graphitized basal plane which favorably assist in the improvement of catalytic activity and durability of supported nanocatalysts. The novel properties of OMCs such as high surface area and large amount of mesopores facilitate high metal dispersion and good reactant flux rendering it a highly suitable electrocatalyst support for fuel cells. Moreover, the defects and functional groups present on the surface of OMCs act as sites for deposition of metal nanocatalysts and metal–support interaction resulting in improved activity and durability of OMC-based hybrid catalysts. Biomass offers sustainable and renewable resources for derivation of novel "green carbon" materials as electrocatalyst support materials. Most often, biomass derived carbon materials are self-heteroatom doped which favorably enhance the electrocatalytic activity. Though significant advances have been made in the synthesis of graphene, OMCs, and green carbon, it is vital to develop simpler, more effective, and low cost procedure for their mass production. Furthermore, most of the electrocatalytic and stability measurements with newly developed carbonaceous nanostructures are carried out in half-cell mode (RDE) with acidic/alkaline electrolytes which are not true representation of their actual

performance in fuel cell. Hence, it is essential to evaluate their performance in-situ in working fuel cell under operating conditions to validate their practical applicability. It is certain that continued concerted research in this exciting field of new carbonaceous materials will help to alleviate the limitations of low-temperature fuel cells and result in enhanced performance for wide scale commercial applications.

Acknowledgments The authors gratefully acknowledge Director, VSSC and Deputy Director, PCM, VSSC for granting permission to publish this work.

References

1. Wang Y, Chen KS, Mishler J, Cho SC, Adroher XC (2011) A review of polymer electrolyte membrane fuel cells: technology, applications, and needs on fundamental research. Appl Energy 88(4):981–1007
2. Sharaf OZ, Orhan MF (2014) An overview of fuel cell technology: fundamentals and applications. Renew Sust Energ Rev 32:810–853
3. Wilberforce T, Alaswad A, Palumbo A, Dassisti M, Olabi AG (2016) Advances in stationary and portable fuel cell applications. Int J Hydrog Energy 41(37):16509–16522
4. O'Hayre R, Cha S-W, Prinz FB, Colella W (2016) Fuel cell fundamentals. Wiley, Hoboken
5. Dicks AL, Rand DAJ (2018) Fuel cell systems explained. Wiley, New York
6. Liu M, Zhang R, Chen W (2014) Graphene-supported nanoelectrocatalysts for fuel cells: synthesis, properties, and applications. Chem Rev 114(10):5117–5160
7. Sharma S, Pollet BG (2012) Support materials for PEMFC and DMFC electrocatalysts—a review. J Power Sources 208:96–119
8. Basri S, Kamarudin SK, Daud WRW, Yaakub Z (2010) Nanocatalyst for direct methanol fuel cell (DMFC). Int J Hydrog Energy 35(15):7957–7970
9. Huang H, Wang X (2014) Recent progress on carbon-based support materials for electrocatalysts of direct methanol fuel cells. J Mater Chem A 2(18):6266–6291
10. Bharti A, Cheruvally G (2017) Influence of various carbon nano-forms as supports for Pt catalyst on proton exchange membrane fuel cell performance. J Power Sources 360:196–205
11. Yuan X, Ding X-L, Wang C-Y, Ma Z-F (2013) Use of polypyrrole in catalysts for low temperature fuel cells. Energy Environ Sci 6(4):1105–1124
12. Xu JB, Zhao TS (2013) Mesoporous carbon with uniquely combined electrochemical and mass transport characteristics for polymer electrolyte membrane fuel cells. RSC Adv 3 (1):16–24
13. Antolini E (2016) Nitrogen-doped carbons by sustainable N-and C-containing natural resources as nonprecious catalysts and catalyst supports for low temperature fuel cells. Renew Sust Energ Rev 58:34–51
14. Dhakate SR, Chauhan N, Sharma S, Tawale J, Singh S, Sahare PD, Mathur RB (2011) An approach to produce single and double layer graphene from re-exfoliation of expanded graphite. Carbon 49(6):1946–1954
15. Qu L, Liu Y, Baek J-B, Dai L (2010) Nitrogen-doped graphene as efficient metal-free electrocatalyst for oxygen reduction in fuel cells. ACS Nano 4(3):1321–1326
16. Novoselov KS, Geim AK, Morozov SV, Jiang D, Zhang Y, Dubonos SV, Grigorieva IV, Firsov AA (2004) Electric field effect in atomically thin carbon films. Science 306 (5696):666–669
17. Yin PT, Shah S, Chhowalla M, Lee K-B (2015) Design, synthesis, and characterization of graphene–nanoparticle hybrid materials for bioapplications. Chem Rev 115(7):2483–2531

18. Randviir EP, Brownson DAC, Banks CE (2014) A decade of graphene research: production, applications and outlook. Mater Today 17(9):426–432
19. Zhong YL, Tian Z, Simon GP, Li D (2015) Scalable production of graphene via wet chemistry: progress and challenges. Mater Today 18(2):73–78
20. Avouris P, Dimitrakopoulos C (2012) Graphene: synthesis and applications. Mater Today 15 (3):86–97
21. Edwards RS, Coleman KS (2013) Graphene synthesis: relationship to applications. Nanoscale 5(1):38–51
22. Selvakumar D, Tripathi SK, Singh R, Nasim M (2007) Solvo-thermal preparation of cadmium telluride nanoparticles from a novel single source molecular precursor. Chem Lett 37(1):34–35
23. Das S, Sudhagar P, Kang YS, Choi W (2014) Graphene synthesis and application for solar cells. J Mater Res 29(3):299–319
24. Yi M, Shen Z (2015) A review on mechanical exfoliation for the scalable production of graphene. J Mater Chem A 3(22):11700–11715
25. Van Noorden R (2012) Production: beyond sticky tape. Nature 483:S32. https://doi.org/10.1038/483S32a
26. Dresselhaus MS, Dresselhaus G (2002) Intercalation compounds of graphite. Adv Phys 51 (1):1–186
27. Jayasena B, Subbiah S (2011) A novel mechanical cleavage method for synthesizing few-layer graphenes. Nanoscale Res Lett 6(1):95
28. Chen J, Duan M, Chen G (2012) Continuous mechanical exfoliation of graphene sheets via three-roll mill. J Mater Chem 22(37):19625–19628
29. Muñoz R, Gómez-Aleixandre C (2013) Review of CVD synthesis of graphene. Chem Vap Depos 19:297–322
30. Wu W, Liu Z, Jauregui LA, Yu Q, Pillai R, Cao H, Bao J, Chen YP, Pei S-S (2010) Wafer-scale synthesis of graphene by chemical vapor deposition and its application in hydrogen sensing. Sensor Actuat B Chem 150(1):296–300
31. Van Nang L, Kim E-T (2012) Controllable synthesis of high-quality graphene using inductively-coupled plasma chemical vapor deposition. J Electrochem Soc 159(4):K93–K96
32. Chae SJ, Güneş F, Kim KK, Kim ES, Han GH, Kim SM, Shin HJ, Yoon SM, Choi JY, Park MH (2009) Synthesis of large-area graphene layers on poly-nickel substrate by chemical vapor deposition: wrinkle formation. Adv Mater 21(22):2328–2333
33. Hummers WS Jr, Offeman RE (1958) Preparation of graphitic oxide. J Am Chem Soc 80 (6):1339–1339
34. Iqbal MZ, Abdala AA (2013) Thermally reduced graphene: synthesis, characterization and dye removal applications. RSC Adv 3(46):24455–24464
35. Staudenmaier L (1898) Verfahren zur darstellung der graphitsäure. Eur J Inorg Chem 31 (2):1481–1487
36. Choi SM, Seo MH, Kim HJ, Kim WB (2011) Synthesis of surface-functionalized graphene nanosheets with high Pt-loadings and their applications to methanol electrooxidation. Carbon 49(3):904–909
37. Kaniyoor A, Baby TT, Ramaprabhu S (2010) Graphene synthesis via hydrogen induced low temperature exfoliation of graphite oxide. J Mater Chem 20(39):8467–8469
38. Yan J, Wang Q, Wei T, Jiang L, Zhang M, Jing X, Fan Z (2014) Template-assisted low temperature synthesis of functionalized graphene for ultrahigh volumetric performance supercapacitors. ACS Nano 8(5):4720–4729
39. Antolini E (2012) Graphene as a new carbon support for low-temperature fuel cell catalysts. Appl Catal B Environ 123:52–68
40. Sheng Z-H, Shao L, Chen J-J, Bao W-J, Wang F-B, Xia X-H (2011) Catalyst-free synthesis of nitrogen-doped graphene via thermal annealing graphite oxide with melamine and its excellent electrocatalysis. ACS Nano 5(6):4350–4358

41. Stankovich S, Dikin DA, Piner RD, Kohlhaas KA, Kleinhammes A, Jia Y, Wu Y, Nguyen ST, Ruoff RS (2007) Synthesis of graphene-based nanosheets via chemical reduction of exfoliated graphite oxide. Carbon 45(7):1558–1565
42. Ramachandran R, Saranya M, Velmurugan V, Raghupathy BPC, Jeong SK, Grace AN (2015) Effect of reducing agent on graphene synthesis and its influence on charge storage towards supercapacitor applications. Appl Energy 153:22–31
43. Sridhar V, Jeon J-H, Oh I-K (2010) Synthesis of graphene nano-sheets using eco-friendly chemicals and microwave radiation. Carbon 48(10):2953–2957
44. Wang Y, Shi Z, Yin J (2011) Facile synthesis of soluble graphene via a green reduction of graphene oxide in tea solution and its biocomposites. ACS Appl Mater Interfaces 3 (4):1127–1133
45. Toh SY, Loh KS, Kamarudin SK, Daud WRW (2014) Graphene production via electrochemical reduction of graphene oxide: synthesis and characterisation. Chem Eng J 251:422–434
46. Alanyalıoğlu M, Segura JJ, Oro-Sole J, Casan-Pastor N (2012) The synthesis of graphene sheets with controlled thickness and order using surfactant-assisted electrochemical processes. Carbon 50(1):142–152
47. Wang G, Wang B, Park J, Wang Y, Sun B, Yao J (2009) Highly efficient and large-scale synthesis of graphene by electrolytic exfoliation. Carbon 47(14):3242–3246
48. Cooper AJ, Wilson NR, Kinloch IA, Dryfe RAW (2014) Single stage electrochemical exfoliation method for the production of few-layer graphene via intercalation of tetraalkylammonium cations. Carbon 66:340–350
49. Li Y, Tang L, Li J (2009) Preparation and electrochemical performance for methanol oxidation of Pt/graphene nanocomposites. Electrochem Commun 11(4):846–849
50. Jafri RI, Rajalakshmi N, Ramaprabhu S (2010) Nitrogen doped graphene nanoplatelets as catalyst support for oxygen reduction reaction in proton exchange membrane fuel cell. J Mater Chem 20(34):7114–7117
51. Hsieh SH, Hsu MC, Liu WL, Chen WJ (2013) Study of Pt catalyst on graphene and its application to fuel cell. Appl Surf Sci 277:223–230
52. Galema SA (1997) Microwave chemistry. Chem Soc Rev 26(3):233–238
53. Bharti A, Cheruvally G, Muliankeezhu S (2017) Microwave assisted, facile synthesis of Pt/CNT catalyst for proton exchange membrane fuel cell application. Int J Hydrog Energy 42(16):11622–11631
54. Zhao L, Wang Z-B, Li J-L, Zhang J-J, Sui X-L, Zhang L-M (2015) A newly-designed sandwich-structured graphene–Pt–graphene catalyst with improved electrocatalytic performance for fuel cells. J Mater Chem A 3(10):5313–5320
55. Pullamsetty A, Sundara R (2016) Investigation of catalytic activity towards oxygen reduction reaction of Pt dispersed on boron doped graphene in acid medium. J Colloid Interface Sci 479:260–270
56. Pullamsetty A, Subbiah M, Sundara R (2015) Platinum on boron doped graphene as cathode electrocatalyst for proton exchange membrane fuel cells. Int J Hydrog Energy 40 (32):10251–10261
57. Oztuna FES, Barim SB, Bozbag SE, Yu H, Aindow M, Unal U, Erkey C (2017) Graphene aerogel supported Pt electrocatalysts for oxygen reduction reaction by supercritical deposition. Electrochim Acta 250:174–184
58. Daş E, Gürsel SA, Şanli LI, Yurtcan AB (2016) Comparison of two different catalyst preparation methods for graphene nanoplatelets supported platinum catalysts. Int J Hydrog Energy 41(23):9755–9761
59. Liu S, Wang J, Zeng J, Ou J, Li Z, Liu X, Yang S (2010) "Green" electrochemical synthesis of Pt/graphene sheet nanocomposite film and its electrocatalytic property. J Power Sources 195 (15):4628–4633
60. Zhu J, Xiao M, Zhao X, Liu C, Ge J, Xing W (2015) Strongly coupled Pt nanotubes/N-doped graphene as highly active and durable electrocatalysts for oxygen reduction reaction. Nano Energy 13:318–326

61. Guo S, Dong S, Wang E (2009) Three-dimensional Pt-on-Pd bimetallic nanodendrites supported on graphene nanosheet: facile synthesis and used as an advanced nanoelectrocatalyst for methanol oxidation. ACS Nano 4(1):547–555
62. Jafri RI, Rajalakshmi N, Dhathathreyan KS, Ramaprabhu S (2015) Nitrogen doped graphene prepared by hydrothermal and thermal solid state methods as catalyst supports for fuel cell. Int J Hydrog Energy 40(12):4337–4348
63. Ryoo R, Joo SH, Jun S (1999) Synthesis of highly ordered carbon molecular sieves via template-mediated structural transformation. J Phys Chem B 103(37):7743–7746
64. Eftekhari A, Fan Z (2017) Ordered mesoporous carbon and its applications for electrochemical energy storage and conversion. Mater Chem Front 1(6):1001–1027
65. Ambrosio EP, Francia C, Manzoli M, Penazzi N, Spinelli P (2008) Platinum catalyst supported on mesoporous carbon for PEMFC. Int J Hydrog Energy 33(12):3142–3145
66. Ryoo R, Joo SH, Kruk M, Jaroniec M (2001) Ordered mesoporous carbons. Adv Mater 13 (9):677–681
67. Ryoo R, Joo SH (2004) Nanostructured carbon materials synthesized from mesoporous silica crystals by replication. Stud Surf Sci Catal 148:241–260
68. Lee J, Han S, Hyeon T (2004) Synthesis of new nanoporous carbon materials using nano-structured silica materials as templates. J Mater Chem 14(4):478–486
69. Yang H, Zhao D (2005) Synthesis of replica mesostructures by the nanocasting strategy. J Mater Chem 15(12):1217–1231
70. Lu AH, Schüth F (2006) Nanocasting: a versatile strategy for creating nanostructured porous materials. Adv Mater 18(14):1793–1805
71. Lee J, Kim J, Hyeon T (2006) Recent progress in the synthesis of porous carbon materials. Adv Mater 18(16):2073–2094
72. Chang H, Joo SH, Pak C (2007) Synthesis and characterization of mesoporous carbon for fuel cell applications. J Mater Chem 17(30):3078–3088
73. Xu W, Wu Z, Tao S (2016) Recent progress in electrocatalysts with mesoporous structures for application in polymer electrolyte membrane fuel cells. J Mater Chem A 4(42):16272–16287
74. Deng Y, Wei J, Sun Z, Zhao D (2013) Large-pore ordered mesoporous materials templated from non-Pluronic amphiphilic block copolymers. Chem Soc Rev 42(9):4054–4070
75. Antolini E (2009) Carbon supports for low-temperature fuel cell catalysts. Appl Catal B Environ 88(1–2):1–24
76. Morishita T, Tsumura T, Toyoda M, Przepiórski J, Morawski AW, Konno H, Inagaki M (2010) A review of the control of pore structure in MgO-templated nanoporous carbons. Carbon 48(10):2690–2707
77. Liang C, Li Z, Dai S (2008) Mesoporous carbon materials: synthesis and modification. Angew Chem Int Ed Engl 47(20):3696–3717
78. Joo SH, Choi SJ, Oh I, Kwak J, Liu Z, Terasaki O, Ryoo R (2001) Ordered nanoporous arrays of carbon supporting high dispersions of platinum nanoparticles. Nature 412(6843):169
79. Li Z, Jaroniec M (2001) Colloidal imprinting: a novel approach to the synthesis of mesoporous carbons. J Am Chem Soc 123(37):9208–9209
80. Li Z, Jaroniec M (2001) Silica gel-templated mesoporous carbons prepared from mesophase pitch and polyacrylonitrile. Carbon 39(13):2080–2082
81. Li Z, Jaroniec M (2003) Synthesis and adsorption properties of colloid-imprinted carbons with surface and volume mesoporosity. Chem Mater 15(6):1327–1333
82. Jun S, Joo SH, Ryoo R, Kruk M, Jaroniec M, Liu Z, Ohsuna T, Terasaki O (2000) Synthesis of new, nanoporous carbon with hexagonally ordered mesostructure. J Am Chem Soc 122 (43):10712–10713
83. Banham D, Feng F, Burt J, Alsrayheen E, Birss V (2010) Bimodal, templated mesoporous carbons for capacitor applications. Carbon 48(4):1056–1063
84. Kim CH, Lee D-K, Pinnavaia TJ (2004) Graphitic mesostructured carbon prepared from aromatic precursors. Langmuir 20(13):5157–5159

85. Banham D, Feng F, Pei K, Ye S, Birss V (2013) Effect of carbon support nanostructure on the oxygen reduction activity of Pt/C catalysts. J Mater Chem A 1(8):2812–2820
86. Zhai Y, Wan Y, Cheng Y, Shi Y, Zhang F, Tu B, Zhao D (2008) The influence of carbon source on the wall structure of ordered mesoporous carbons. J Porous Mater 15(5):601–611
87. Li X, Forouzandeh F, Fürstenhaupt T, Banham D, Feng F, Ye S, Kwok DY, Birss V (2018) New insights into the surface properties of hard-templated ordered mesoporous carbons. Carbon 127:707–717
88. Lei Z, Xiao Y, Dang L, Lu M, You W (2006) Fabrication of ultra-large mesoporous carbon with tunable pore size by monodisperse silica particles derived from seed growth process. Microporous Mesoporous Mater 96(1–3):127–134
89. Zhang S, Chen L, Zhou S, Zhao D, Wu L (2010) Facile synthesis of hierarchically ordered porous carbon via in situ self-assembly of colloidal polymer and silica spheres and its use as a catalyst support. Chem Mater 22(11):3433–3440
90. Li Y, Yang Y, Shi J, Ruan M (2008) Synthesis and characterization of hollow mesoporous carbon spheres with a highly ordered bicontinuous cubic mesostructure. Microporous Mesoporous Mater 112(1–3):597–602
91. Gierszal KP, Jaroniec M (2006) Carbons with extremely large volume of uniform mesopores synthesized by carbonization of phenolic resin film formed on colloidal silica template. J Am Chem Soc 128(31):10026–10027
92. Chuenchom L, Kraehnert R, Smarsly BM (2012) Recent progress in soft-templating of porous carbon materials. Soft Matter 8(42):10801–10812
93. Wang Q, Zhang W, Mu Y, Zhong L, Meng Y, Sun Y (2014) Synthesis of ordered mesoporous carbons with tunable pore size by varying carbon precursors via soft-template method. Microporous Mesoporous Mater 197:109–115
94. de Aa Soler-Illia GJ, Crepaldi EL, Grosso D, Sanchez C (2003) Block copolymer-templated mesoporous oxides. Curr Opin Colloid Interface Sci 8(1):109–126
95. Wan Y, Zhao D (2007) On the controllable soft-templating approach to mesoporous silicates. Chem Rev 107(7):2821–2860
96. Wan Y, Shi Y, Zhao D (2007) Supramolecular aggregates as templates: ordered mesoporous polymers and carbons. Chem Mater 20(3):932–945
97. Ma T-Y, Liu L, Yuan Z-Y (2013) Direct synthesis of ordered mesoporous carbons. Chem Soc Rev 42(9):3977–4003
98. Zhang F, Meng Y, Gu D, Yan Y, Chen Z, Tu B, Zhao D (2006) An aqueous cooperative assembly route to synthesize ordered mesoporous carbons with controlled structures and morphology. Chem Mater 18(22):5279–5288
99. Meng Y, Gu D, Zhang F, Shi Y, Yang H, Li Z, Yu C, Tu B, Zhao D (2005) Ordered mesoporous polymers and homologous carbon frameworks: amphiphilic surfactant templating and direct transformation. Angew Chem Int Ed Engl 117(43):7215–7221
100. Hillmyer MA, Bates FS, Almdal K, Mortensen K, Ryan AJ, Fairclough JPA (1996) Complex phase behavior in solvent-free nonionic surfactants. Science 271(5251):976–978
101. Bucknall DG, Anderson HL (2003) Polymers get organized. Science 302(5652):1904–1905
102. Sanchez C, Boissiere C, Grosso D, Laberty C, Nicole L (2008) Design, synthesis, and properties of inorganic and hybrid thin films having periodically organized nanoporosity. Chem Mater 20(3):682–737
103. Liang C, Hong K, Guiochon GA, Mays JW, Dai S (2004) Synthesis of a large-scale highly ordered porous carbon film by self-assembly of block copolymers. Angew Chem Int Ed Engl 43(43):5785–5789
104. Tanaka S, Nishiyama N, Egashira Y, Ueyama K (2005) Synthesis of ordered mesoporous carbons with channel structure from an organic–organic nanocomposite. Chem Commun (16):2125–2127
105. Meng Y, Gu D, Zhang F, Shi Y, Cheng L, Feng D, Wu Z, Chen Z, Wan Y, Stein A (2006) A family of highly ordered mesoporous polymer resin and carbon structures from organic–organic self-assembly. Chem Mater 18(18):4447–4464

106. Wang Y, He C, Brouzgou A, Liang Y, Fu R, Wu D, Tsiakaras P, Song S (2012) A facile soft-template synthesis of ordered mesoporous carbon/tungsten carbide composites with high surface area for methanol electrooxidation. J Power Sources 200:8–13
107. Zhao G, Zhao TS, Xu J, Lin Z, Yan X (2017) Impact of pore size of ordered mesoporous carbon FDU-15-supported platinum catalysts on oxygen reduction reaction. Int J Hydrog Energy 42(5):3325–3334
108. Wan Y, Shi Y, Zhao D (2007) Designed synthesis of mesoporous solids via nonionic-surfactant-templating approach. Chem Commun (9):897–926
109. Yu C, Fan J, Tian B, Stucky GD, Zhao D (2003) Synthesis of mesoporous silica from commercial poly (ethylene oxide)/poly (butylene oxide) copolymers: toward the rational design of ordered mesoporous materials. J Phys Chem B 107(48):13368–13375
110. Wan Y, Shi Y, Zhao D (2008) Ordered mesoporous polymers and carbon molecular sieves. Chem Mater 20:932–945
111. Deng Y, Yu T, Wan Y, Shi Y, Meng Y, Gu D, Zhang L, Huang Y, Liu C, Wu X (2007) Ordered mesoporous silicas and carbons with large accessible pores templated from amphiphilic diblock copolymer poly (ethylene oxide)-b-polystyrene. J Am Chem Soc 129 (6):1690–1697
112. Deng Y, Liu C, Gu D, Yu T, Tu B, Zhao D (2008) Thick wall mesoporous carbons with a large pore structure templated from a weakly hydrophobic PEO–PMMA diblock copolymer. J Mater Chem 18(1):91–97
113. Li W, Liu J, Zhao D (2016) Mesoporous materials for energy conversion and storage devices. Nat Rev Mater 1(6):16023
114. Liu H, Song C, Zhang L, Zhang J, Wang H, Wilkinson DP (2006) A review of anode catalysis in the direct methanol fuel cell. J Power Sources 155(2):95–110
115. Shen W, Li Z, Liu Y (2008) Surface chemical functional groups modification of porous carbon. Recent Pat Chem Eng 1(1):27–40
116. Tang J, Liu J, Torad NL, Kimura T, Yamauchi Y (2014) Tailored design of functional nanoporous carbon materials toward fuel cell applications. Nano Today 9(3):305–323
117. Guha A, Lu W, Zawodzinski TA Jr, Schiraldi DA (2007) Surface-modified carbons as platinum catalyst support for PEM fuel cells. Carbon 45(7):1506–1517
118. Salgado JRC, Quintana JJ, Calvillo L, Lázaro MJ, Cabot PL, Esparbé I, Pastor E (2008) Carbon monoxide and methanol oxidation at platinum catalysts supported on ordered mesoporous carbon: the influence of functionalization of the support. Phys Chem Chem Phys 10(45):6796–6806
119. Perini L, Durante C, Favaro M, Perazzolo V, Agnoli S, Schneider O, Granozzi G, Gennaro A (2015) Metal–support interaction in platinum and palladium nanoparticles loaded on nitrogen-doped mesoporous carbon for oxygen reduction reaction. ACS Appl Mater Interfaces 7 (2):1170–1179
120. Xiao C, Chen X, Fan Z, Liang J, Zhang B, Ding S (2016) Surface-nitrogen-rich ordered mesoporous carbon as an efficient metal-free electrocatalyst for oxygen reduction reaction. Nanotechnology 27(44):445402
121. Ji X, Lee KT, Holden R, Zhang L, Zhang J, Botton GA, Couillard M, Nazar LF (2010) Nanocrystalline intermetallics on mesoporous carbon for direct formic acid fuel cell anodes. Nat Chem 2(4):286
122. Zhou J-H, He J-P, Ji Y-J, Dang W-J, Liu X-L, Zhao G-W, Zhang C-X, Zhao J-S, Fu Q-B, Hu H-P (2007) CTAB assisted microwave synthesis of ordered mesoporous carbon supported Pt nanoparticles for hydrogen electro-oxidation. Electrochim Acta 52(14):4691–4695
123. Li F, Wang H, Zhao X, Li B, Zhang Y (2016) Microwave-assisted route for the preparation of Pd anchored on surfactant functionalized ordered mesoporous carbon and its electrochemical applications. RSC Adv 6(75):70810–70815
124. Zhang Y, Bo X, Luhana C, Guo L (2011) Preparation and electrocatalytic application of high dispersed Pt nanoparticles/ordered mesoporous carbon composites. Electrochim Acta 56 (17):5849–5854

125. Momčilović M, Stojmenović M, Gavrilov N, Pašti I, Mentus S, Babić B (2014) Complex electrochemical investigation of ordered mesoporous carbon synthesized by soft-templating method: charge storage and electrocatalytical or Pt-electrocatalyst supporting behavior. Electrochim Acta 125:606–614
126. Cao J, Chen Z, Xu J, Wang W, Chen Z (2013) Mesoporous carbon synthesized from dual colloidal silica/block copolymer template approach as the support of platinum nanoparticles for direct methanol fuel cells. Electrochim Acta 88:184–192
127. Zhang C, Xu L, Shan N, Sun T, Chen J, Yan Y (2014) Enhanced electrocatalytic activity and durability of Pt particles supported on ordered mesoporous carbon spheres. ACS Catal 4 (6):1926–1930
128. Joo SH, Kwon K, You DJ, Pak C, Chang H, Kim JM (2009) Preparation of high loading Pt nanoparticles on ordered mesoporous carbon with a controlled Pt size and its effects on oxygen reduction and methanol oxidation reactions. Electrochim Acta 54(24):5746–5753
129. Joo SH, Lee HI, You DJ, Kwon K, Kim JH, Choi YS, Kang M, Kim JM, Pak C, Chang H (2008) Ordered mesoporous carbons with controlled particle sizes as catalyst supports for direct methanol fuel cell cathodes. Carbon 46(15):2034–2045
130. Ahn C-Y, Cheon J-Y, Joo S-H, Kim J (2013) Effects of ionomer content on Pt catalyst/ordered mesoporous carbon support in polymer electrolyte membrane fuel cells. J Power Sources 222:477–482
131. Kim N-I, Cheon JY, Kim JH, Seong J, Park J-Y, Joo SH, Kwon K (2014) Impact of framework structure of ordered mesoporous carbons on the performance of supported Pt catalysts for oxygen reduction reaction. Carbon 72:354–364
132. Calvillo L, Lázaro MJ, García-Bordejé E, Moliner R, Cabot PL, Esparbé I, Pastor E, Quintana JJ (2007) Platinum supported on functionalized ordered mesoporous carbon as electrocatalyst for direct methanol fuel cells. J Power Sources 169(1):59–64
133. Morales-Acosta D, Rodríguez-Varela FJ, Benavides R (2016) Template-free synthesis of ordered mesoporous carbon: application as support of highly active Pt nanoparticles for the oxidation of organic fuels. Int J Hydrog Energy 41(5):3387–3398
134. Samiee L, Shoghi F, Maghsodi A (2014) In situ functionalisation of mesoporous carbon electrodes with carbon nanotubes for proton exchange membrane fuel-cell application. Mater Chem Phys 143(3):1228–1235
135. Nsabimana A, Bo X, Zhang Y, Li M, Han C, Guo L (2014) Electrochemical properties of boron-doped ordered mesoporous carbon as electrocatalyst and Pt catalyst support. J Colloid Interface Sci 428:133–140
136. Song P, Zhu L, Bo X, Wang A, Wang G, Guo L (2014) Pt nanoparticles incorporated into phosphorus-doped ordered mesoporous carbons: enhanced catalytic activity for methanol electrooxidation. Electrochim Acta 127:307–314
137. Bruno MM, Petruccelli MA, Viva FA, Corti HR (2013) Mesoporous carbon supported PtRu as anode catalyst for direct methanol fuel cell: polarization measurements and electrochemical impedance analysis of mass transport. Int J Hydrog Energy 38(10):4116–4123
138. Hung C-T, Liou Z-H, Veerakumar P, Wu P-H, Liu T-C, Liu S-B (2016) Ordered mesoporous carbon supported bifunctional PtM (M= Ru, Fe, Mo) electrocatalysts for a fuel cell anode. Chin J Catal 37(1):43–53
139. Volotskova O, Levchenko I, Shashurin A, Raitses Y, Ostrikov K, Keidar M (2010) Single-step synthesis and magnetic separation of graphene and carbon nanotubes in arc discharge plasmas. Nanoscale 2(10):2281–2285
140. Li X, Cai W, An J, Kim S, Nah J, Yang D, Piner R, Velamakanni A, Jung I, Tutuc E (2009) Large-area synthesis of high-quality and uniform graphene films on copper foils. Science 324 (5932):1312–1314
141. Titirici M-M, White RJ, Falco C, Sevilla M (2012) Black perspectives for a green future: hydrothermal carbons for environment protection and energy storage. Energy Environ Sci 5 (5):6796–6822

142. Wei L, Sevilla M, Fuertes AB, Mokaya R, Yushin G (2011) Hydrothermal carbonization of abundant renewable natural organic chemicals for high-performance supercapacitor electrodes. Adv Energy Mater 1(3):356–361
143. Liu W-J, Jiang H, Yu H-Q (2015) Development of biochar-based functional materials: toward a sustainable platform carbon material. Chem Rev 115(22):12251–12285
144. Falco C, Baccile N, Titirici M-M (2011) Morphological and structural differences between glucose, cellulose and lignocellulosic biomass derived hydrothermal carbons. Green Chem 13 (11):3273–3281
145. Fellinger TP, White RJ, Titirici MM, Antonietti M (2012) Borax-mediated formation of carbon aerogels from glucose. Adv Funct Mater 22(15):3254–3260
146. Liu X, Antonietti M (2014) Molten salt activation for synthesis of porous carbon nanostructures and carbon sheets. Carbon 69:460–466
147. Xiao Y, Dong H, Lei B, Qiu H, Liu Y, Zheng M (2015) Ordered mesoporous carbons with fiber-and rod-like morphologies for supercapacitor electrode materials. Mater Lett 138:37–40
148. Ting C-C, Wu H-Y, Vetrivel S, Saikia D, Pan Y-C, Fey GTK, Kao H-M (2010) A one-pot route to synthesize highly ordered mesoporous carbons and silicas through organic–inorganic self-assembly of triblock copolymer, sucrose and silica. Microporous Mesoporous Mater 128 (1–3):1–11
149. Sivadas DL, Vijayan S, Rajeev R, Ninan KN, Prabhakaran K (2016) Nitrogen-enriched microporous carbon derived from sucrose and urea with superior CO_2 capture performance. Carbon 109:7–18
150. Yu L, Brun N, Sakaushi K, Eckert J, Titirici MM (2013) Hydrothermal nanocasting: synthesis of hierarchically porous carbon monoliths and their application in lithium–sulfur batteries. Carbon 61:245–253
151. Yu L, Falco C, Weber J, White RJ, Howe JY, Titirici M-M (2012) Carbohydrate-derived hydrothermal carbons: a thorough characterization study. Langmuir 28(33):12373–12383
152. Wu Z-Y, Liang H-W, Chen L-F, Hu B-C, Yu S-H (2015) Bacterial cellulose: a robust platform for design of three dimensional carbon-based functional nanomaterials. Acc Chem Res 49 (1):96–105
153. Klemm D, Kramer F, Moritz S, Lindström T, Ankerfors M, Gray D, Dorris A (2011) Nanocelluloses: a new family of nature-based materials. Angew Chem Int Ed Engl 50 (24):5438–5466
154. Liu Q, Chen C, Pan F, Zhang J (2015) Highly efficient oxygen reduction on porous nitrogen-doped nanocarbons directly synthesized from cellulose nanocrystals and urea. Electrochim Acta 170:234–241
155. Li S, Xu W, Cheng P, Luo J, Zhou D, Li J, Li R, Yuan D (2017) Bacterial cellulose derived iron and phosphorus co-doped carbon nanofibers as an efficient oxygen reduction reaction electrocatalysts. Synth Met 223:137–144
156. Liang H-W, Wu Z-Y, Chen L-F, Li C, Yu S-H (2015) Bacterial cellulose derived nitrogen-doped carbon nanofiber aerogel: an efficient metal-free oxygen reduction electrocatalyst for zinc-air battery. Nano Energy 11:366–376
157. Lai F, Miao YE, Zuo L, Lu H, Huang Y, Liu T (2016) Biomass-derived nitrogen-doped carbon nanofiber network: a facile template for decoration of ultrathin nickel-cobalt layered double hydroxide nanosheets as high-performance asymmetric supercapacitor electrode. Small 12 (24):3235–3244
158. Mulyadi A, Zhang Z, Dutzer M, Liu W, Deng Y (2017) Facile approach for synthesis of doped carbon electrocatalyst from cellulose nanofibrils toward high-performance metal-free oxygen reduction and hydrogen evolution. Nano Energy 32:336–346
159. Wu Z-Y, Liang H-W, Li C, Hu B-C, Xu X-X, Wang Q, Chen J-F, Yu S-H (2014) Dyeing bacterial cellulose pellicles for energetic heteroatom doped carbon nanofiber aerogels. Nano Res 7(12):1861–1872
160. Zu G, Shen J, Zou L, Wang F, Wang X, Zhang Y, Yao X (2016) Nanocellulose-derived highly porous carbon aerogels for supercapacitors. Carbon 99:203–211

161. Sun Y, Wang X, Ding C, Cheng W, Chen C, Hayat T, Alsaedi A, Hu J, Wang X (2016) Direct synthesis of bacteria-derived carbonaceous nanofibers as a highly efficient material for radionuclides elimination. ACS Sustain Chem Eng 4(9):4608–4616
162. Wu Z-Y, Hu B-C, Wu P, Liang H-W, Yu Z-L, Lin Y, Zheng Y-R, Li Z, Yu S-H (2016) Mo 2 C nanoparticles embedded within bacterial cellulose-derived 3D N-doped carbon nanofiber networks for efficient hydrogen evolution. NPG Asia Mater 8(7):e288
163. Rybarczyk MK, Gontarek E, Lieder M, Titirici M-M (2018) Salt melt synthesis of curved nitrogen-doped carbon nanostructures: ORR kinetics boost. Appl Surf Sci 435:543–551
164. Kucinska A, Golembiewski R, Lukaszewicz JP (2014) Synthesis of N-rich activated carbons from chitosan by chemical activation. Sci Adv Mater 6(2):290–297
165. Wang Y-Y, Hou B-H, Lü H-Y, Wan F, Wang J, Wu X-L (2015) Porous N-doped carbon material derived from prolific chitosan biomass as a high-performance electrode for energy storage. RSC Adv 5(118):97427–97434
166. Chen P, Wang L-K, Wang G, Gao M-R, Ge J, Yuan W-J, Shen Y-H, Xie A-J, Yu S-H (2014) Nitrogen-doped nanoporous carbon nanosheets derived from plant biomass: an efficient catalyst for oxygen reduction reaction. Energy Environ Sci 7(12):4095–4103
167. Liu X, Zhou Y, Zhou W, Li L, Huang S, Chen S (2015) Biomass-derived nitrogen self-doped porous carbon as effective metal-free catalysts for oxygen reduction reaction. Nanoscale 7 (14):6136–6142
168. Cheng P, Li T, Yu H, Zhi L, Liu Z, Lei Z (2016) Biomass-derived carbon fiber aerogel as a binder-free electrode for high-rate supercapacitors. J Phys Chem C 120(4):2079–2086
169. Song S, Ma F, Wu G, Ma D, Geng W, Wan J (2015) Facile self-templating large scale preparation of biomass-derived 3D hierarchical porous carbon for advanced supercapacitors. J Mater Chem A 3(35):18154–18162
170. Cheng P, Gao S, Zang P, Yang X, Bai Y, Xu H, Liu Z, Lei Z (2015) Hierarchically porous carbon by activation of shiitake mushroom for capacitive energy storage. Carbon 93:315–324
171. Song H, Li H, Wang H, Key J, Ji S, Mao X, Wang R (2014) Chicken bone-derived N-doped porous carbon materials as an oxygen reduction electrocatalyst. Electrochim Acta 147:520–526
172. Wang R, Wang K, Wang Z, Song H, Wang H, Ji S (2015) Pig bones derived N-doped carbon with multi-level pores as electrocatalyst for oxygen reduction. J Power Sources 297:295–301
173. Fang Y, Wang H, Yu H, Peng F (2016) From chicken feather to nitrogen and sulfur co-doped large surface bio-carbon flocs: an efficient electrocatalyst for oxygen reduction reaction. Electrochim Acta 213:273–282
174. Gao A, Guo N, Yan M, Li M, Wang F, Yang R (2018) Hierarchical porous carbon activated by $CaCO_3$ from pigskin collagen for CO_2 and H_2 adsorption. Microporous Mesoporous Mater 260:172–179
175. Guo C, Liao W, Li Z, Chen C (2015) Exploration of the catalytically active site structures of animal biomass-modified on cheap carbon nanospheres for oxygen reduction reaction with high activity, stability and methanol-tolerant performance in alkaline medium. Carbon 85:279–288
176. Wang H, Wang K, Song H, Li H, Ji S, Wang Z, Li S, Wang R (2015) N-doped porous carbon material made from fish-bones and its highly electrocatalytic performance in the oxygen reduction reaction. RSC Adv 5(60):48965–48970
177. Guo C, Hu R, Liao W, Li Z, Sun L, Shi D, Li Y, Chen C (2017) Protein-enriched fish "biowaste" converted to three-dimensional porous carbon nano-network for advanced oxygen reduction electrocatalysis. Electrochim Acta 236:228–238
178. Wu H, Geng J, Ge H, Guo Z, Wang Y, Zheng G (2016) Egg-derived mesoporous carbon microspheres as bifunctional oxygen evolution and oxygen reduction electrocatalysts. Adv Energy Mater 6(20):1600794, 1–8
179. Lu Y, Zhu N, Yin F, Yang T, Wu P, Dang Z, Liu M, Wei X (2017) Biomass-derived heteroatoms-doped mesoporous carbon for efficient oxygen reduction in microbial fuel cells. Biosens Bioelectron 98:350–356

180. Shao Z, Zhang W, An D, Zhang G, Wang Y (2015) Pyrolyzed egg yolk as an efficient bifunctional electrocatalyst for oxygen reduction and evolution reactions. RSC Adv 5 (118):97508–97511
181. Chaudhari KN, Song MY, Yu JS (2014) Transforming hair into heteroatom-doped carbon with high surface area. Small 10(13):2625–2636
182. Zhao Z-Q, Xiao P-W, Zhao L, Liu Y, Han B-H (2015) Human hair-derived nitrogen and sulfur co-doped porous carbon materials for gas adsorption. RSC Adv 5(90):73980–73988
183. Liu X, Zhou W, Yang L, Li L, Zhang Z, Ke Y, Chen S (2015) Correction: nitrogen and sulfur co-doped porous carbon derived from human hair as highly efficient metal-free electrocatalysts for hydrogen evolution reactions. J Mater Chem A 3(18):10135–10135
184. Ding W, Li L, Xiong K, Wang Y, Li W, Nie Y, Chen S, Qi X, Wei Z (2015) Shape fixing via salt recrystallization: a morphology-controlled approach to convert nanostructured polymer to carbon nanomaterial as a highly active catalyst for oxygen reduction reaction. J Am Chem Soc 137(16):5414–5420
185. Liang J, Du X, Gibson C, Du XW, Qiao SZ (2013) N-doped graphene natively grown on hierarchical ordered porous carbon for enhanced oxygen reduction. Adv Mater 25 (43):6226–6231
186. Gong X, Liu S, Ouyang C, Strasser P, Yang R (2015) Nitrogen-and phosphorus-doped biocarbon with enhanced electrocatalytic activity for oxygen reduction. ACS Catal 5 (2):920–927
187. Ye D, Wang L, Zhang R, Liu B, Wang Y, Kong J (2015) Facile preparation of N-doped mesocellular graphene foam from sludge flocs for highly efficient oxygen reduction reaction. J Mater Chem A 3(29):15171–15176
188. Zhou T, Wang H, Ji S, Linkov V, Wang R (2014) Soybean-derived mesoporous carbon as an effective catalyst support for electrooxidation of methanol. J Power Sources 248:427–433
189. Zhou T, Wang H, Ji S, Feng H, Wang R (2014) Synthesis of mesoporous carbon from okara and application as electrocatalyst support. Fuel Cells 14(2):296–302
190. Zhao X, Zhu J, Liang L, Li C, Liu C, Liao J, Xing W (2014) Biomass-derived N-doped carbon and its application in electrocatalysis. Appl Catal B Environ 154–155:177–182
191. Yan Z, Zhang M, Xie J, Wang H, Wei W (2013) Smaller Pt particles supported on mesoporous bowl-like carbon for highly efficient and stable methanol oxidation and oxygen reduction reaction. J Power Sources 243:48–53
192. Cheng K, Kou Z, Zhang J, Jiang M, Wu H, Hu L, Yang X, Pan M, Mu S (2015) Ultrathin carbon layer stabilized metal catalysts towards oxygen reduction. J Mater Chem A 3 (26):14007–14014
193. Liu H, Cao Y, Wang F, Zhang W, Huang Y (2014) Pig bone derived hierarchical porous carbon-supported platinum nanoparticles with superior electrocatalytic activity towards oxygen reduction reaction. Electroanalysis 26(8):1831–1839
194. Cheng Y, Lu H, Zhang K, Yang F, Dai W, Liu C, Dong H, Zhang X (2018) Fabricating Pt-decorated three dimensional N-doped carbon porous microspherical cavity catalyst for advanced oxygen reduction reaction. Carbon 128:38–45
195. Yang R, Qiu X, Zhang H, Li J, Zhu W, Wang Z, Huang X, Chen L (2005) Monodispersed hard carbon spherules as a catalyst support for the electrooxidation of methanol. Carbon 43 (1):11–16
196. Afraz A, Rafati AA, Hajian A, Khoshnood M (2015) Electrodeposition of Pt nanoparticles on new porous graphitic carbon nanostructures prepared from biomass for fuel cell and methanol sensing applications. Electrocatalysis 6(2):220–228
197. Yang H, Wang H, Ji S, Ma Y, Linkov V, Wang R (2014) Nanostructured Pt supported on cocoon-derived carbon as an efficient electrocatalyst for methanol oxidation. J Solid State Chem 18(6):1503–1512
198. Lobos MLN, Sieben JM, Comignani V, Duarte M, Volpe MA, Moyano EL (2016) Biochar from pyrolysis of cellulose: an alternative catalyst support for the electro-oxidation of methanol. Int J Hydrog Energy 41(25):10695–10706